

Root structure design for hybrid manufacturing of multi-material structures

by

Logan Beguhn

A thesis submitted to the graduate faculty
in partial fulfillment of the requirements for the degree of

MASTER OF SCIENCE

Major: Industrial Engineering

Program of Study Committee:
Frank E. Peters, Major Professor
Matthew C. Frank
Scott Chumbley

The student author, whose presentation of the scholarship herein was approved by the program of study committee, is solely responsible for the content of this thesis. The Graduate College will ensure this thesis is globally accessible and will not permit alterations after a degree is conferred.

Iowa State University

Ames, Iowa

2020

TABLE OF CONTENTS

	Page
LIST OF FIGURES	iii
LIST OF TABLES	vi
NOMENCLATURE	vii
ACKNOWLEDGMENTS	viii
ABSTRACT.....	ix
CHAPTER 1. INTRODUCTION	1
1.1 Overview	1
1.2 Research Motivations and Problems	4
1.3 Organization	4
CHAPTER 2. LITERATURE REVIEW	5
2.1 Hybrid Manufacturing	5
2.2 Big Area Additive Manufacturing	7
2.3 Multi-material parts	9
CHAPTER 3. METHODOLOGY, RESULTS AND DISCUSSION.....	11
3.1 Physical Experimentation	11
3.1.1 Tensile Testing of AM Prints from PE-1 Extruder	11
3.1.2 Tensile Testing of Root Structure Design	17
3.1.3 Shear Tests Across Printing and Substrate Temperatures.....	25
3.2 Theoretical Modeling	29
3.2.1 Dovetail Design.....	30
3.2.2 Lollipop Design.....	37
3.2.3 Thread Design	40
CHAPTER 4. CONCLUSIONS AND FUTURE WORK.....	47
4.1 Conclusions	47
4.2 Limitations and Future Work	49
REFERENCES	51

LIST OF FIGURES

	Page
Figure 1. Process steps to embed polymer into a metallic substrate.....	2
Figure 2. Extruder with 3mm nozzle	11
Figure 3. Material block for tensile testing.....	12
Figure 4. ASTM 638-14 Dimensions for Type 1 Samples [45]	13
Figure 5. Block after waterjet cutting with numbers on samples indicating location they were cut, in decreasing distance from start/stop.....	13
Figure 6. Tensile bar prior to machining in (a) isometric (b) top and (c) left side view	13
Figure 7. (a) Finalized tensile samples and (b) samples during testing	14
Figure 8. Tensile bar samples at (a) 220°C, (b) 250°C, and (c) 280°C	15
Figure 9. Mean tensile stress.....	16
Figure 10. Mean tensile stress with the removal outlier	17
Figure 11. Root structure profile (a) and root cross sections; (b) 20° Dovetail, (c) 40° Dovetail, (d) Lollipop, (e) T-slot, (f) Threaded (inches).....	18
Figure 12. Cross section of (a) 20° Dovetail, (b) 40° Dovetail, (c) Lollipop, (d) T-slot, (e) Threaded root structure geometries	20
Figure 13. Sample testing setup.....	20
Figure 14. (a) Application of acetone, (b) bolting of the assembly	21
Figure 15. Aluminum block bolted to ABS block (Note: all tested samples had two nuts per bolt).....	22
Figure 16. Root structure geometry tensile test	22
Figure 17. (a) 20° dovetail and (b) 40° dovetail	23
Figure 18. Failure modes of (a) Lollipop, (b) T-slot, and (c) Thread root structure design	24
Figure 19. Mean tensile stress.....	25
Figure 20. Schematic of primary bond as the area of concern.....	26

Figure 21. Shear test sample prior to testing, size in Table 4 above.....	27
Figure 22. Block shear test.....	27
Figure 23. Broken shear sample.....	28
Figure 24. Mean shear stress.....	28
Figure 25. 2D cross-section of FEA model	30
Figure 26. Schematic of change in included angle	31
Figure 27. Schematic of (a) 0in. offset, (b) 1/32in. offset, and (c) 1/16in. offset.....	31
Figure 28. Maximum stress vs included angle.....	32
Figure 29. Schematic of change in depth.....	32
Figure 30. (a) tensile test vs (b) shear test	33
Figure 31. Tensile stress as depth of the root structure changes.....	33
Figure 32. Shear stress as depth of the root structure changes	34
Figure 33. (a) Sharp tool point vs. (b) rounded tool	35
Figure 34. Maximum stress of sharp vs. rounded tool tips at 0in. offset.....	36
Figure 35. Maximum stress of sharp and rounded tool tips at 1/32in. offset	36
Figure 36. Drawing of lollipop cutter with varying radii side walls.....	37
Figure 37. Maximum stress versus tool radius	38
Figure 38. Drawing of side walls as stepover changes	39
Figure 39. Stress versus tool stepover.....	39
Figure 40. (a) Single top-down thread vs. (b) single bottom-up thread.....	40
Figure 41. Stress seen in plastic between threads of a top-down vs. bottom-up approach.....	41
Figure 42. Two thread tensile test.....	41
Figure 43. Stress in aluminum substrate and plastic as number of threads increases.....	42
Figure 44. Displacement as the number of threads increase.....	43

Figure 45. (a) Dual threads vs. (b) exterior threads vs. (c) interior threads	44
Figure 46. Maximum stress as thread location changes	45
Figure 47. Change in displacement as the number of threads and thread location change	46

LIST OF TABLES

	Page
Table 1. (a) Printing parameters for block creation and (b) machining parameters	12
Table 2. Root structure cross-section area	22
Table 3. Mean stress results	23
Table 4. Experiment Design	26
Table 5. Dimensions and parameters of shear block samples	26

NOMENCLATURE

ABS	Acrylonitrile Butadiene Styrene
ABS-CF	Acrylonitrile Butadiene Styrene with Carbon Fibers
AM	Additive Manufacturing
ASTM	American Society for Testing and Materials
BAAM	Big Area Additive Manufacturing
CNC	Computer Numerical Control
CTE	Coefficient of Thermal Expansion
FDM	Fused Deposition Modeling
FEA	Finite Element Analysis
LENS	Laser Engineered Net Shaping
NC	Numerical Control
ORNL	Oak Ridge National Laboratory
RP	Rapid Prototyping
SL	Stereolithography
SLS	Selective Laser Sintering
SM	Subtractive Manufacturing
TGA	Thermogravimetric Analysis

ACKNOWLEDGMENTS

First, I would like to thank my major professor, Dr. Frank E. Peters, mentoring me during this journey. Next, I would like to thank my committee members, Dr. Matthew C. Frank and Dr. Scott Chumbley, for their guidance. Without their continual commitment to their students, I would not be completing this work. I would like to recognize Aaron Jordan, Matt Janowicz, and Deb McDonough for their support during my time here. Additionally, I would like to acknowledge my fellow graduate students: Eric Weflen, Sharon Lau, Ali Khorasani, Drew Schweiger, Daniel Schimpf, and Jeffrey Tscherter. Thank you for all your help and encouragement in this process. I also want to thank Sami Larson for laying the groundwork of this project and without it, this project would not be what it is.

I want to take the time to thank former manager and mentor, Corey Magnussen, for encouraging me to pursue higher education in Industrial Engineering. Additionally, I want to thank my managers and mentors during my time at TPI Composites, The Boeing Company and John Deere for giving me the opportunity to learn and grow. Everything I have learned through working in these three different industries has helped me immensely throughout my education. Lastly, I would like to thank my friends, family, and my fiancée for their continued support during this time. Thank you, none of this would be possible without any of you.

ABSTRACT

This research proposes a joining method between a metallic substrate and an additively manufactured (AM) polymer part without the use of adhesives or fasteners. Ideally, a polymer could be extruded onto a metallic substrate with sufficient bond strength; however, due to the characteristics unique to each material, adhesion does not occur. This research investigated an alternative joining method using a root structure of polymer imbedded into the metallic substrate. As the use of hybrid manufacturing methods continues to increase, the proposed method presents an ability to create in-envelope multi-material structures without the need to re-fixture parts.

The objective of this work is to identify a relationship between the design characteristics of the root structure geometry and the strength of the connection. In this work, two different experiment groups were designed to investigate this relationship. The first group utilizes physical experimentation and is broken down into three experiments. First, a baseline of strength was established by creating and testing ASTM 638 samples of material printed via the PE-1 extruder from Hybrid Manufacturing Technologies at three different printing temperatures. Second, five different root structures were created via conventional tools and tensile tested to determine the strength of each root structure. Third, samples were created using one root structure at three different temperatures for both printing and substrate pre-heating to evaluate the effect on shear strength. The second experiment group consists of an FEA investigation to study the effect of root structure geometry and parameter settings on strength. The impact of this work is in providing a new method for joining dissimilar materials in a hybrid manufacturing system and lays the groundwork for a mathematical model to aid in the design of root structure geometries depending on the application of the multi-material system.

CHAPTER 1. INTRODUCTION

This chapter provides an overview of this thesis, research motivation, research problems, and the organization of this document. The overview provides a brief explanation of the system being used in this study, a synopsis of the experiments run, and a summary of the results of the experiments.

1.1 Overview

Hybrid manufacturing is described as the combination of two or more established manufacturing methods into a new cooperative system that utilizes the benefits of each unique manufacturing method [1]. While this definition encompasses a plethora of combinations, this research specifically looks at the utilization of additive and subtractive manufacturing. For this study, a big area additive manufacturing (BAAM) system, classified by the deposition rate, bead size, and the use of pelletized stock, is implemented into a HAAS UMC 750 machining center. This hybrid system combines 5-axis machining capabilities of the UMC 750 with polymer deposition rates upwards of 200x that of desktop printers.

Commonly, most additive manufacturing methods are used to manufacture parts from a single material type, commonly polymers and metals but also ceramics and elastomeric materials. Other systems utilize multiple materials within the same classification; two plastics, two metals, etc. [2]. And some systems, like Selective Laser Sintering (SLS), utilize a composite of two classifications (metal coated in a polymer) to use the polymer to bond the particles together in a green state prior to sintering the metal at a higher temperature [3]. Once the materials become too dissimilar, additional means such as mechanical fasteners or chemical adhesives are needed to join the different materials together. However, there is a lack of research

into alternative methods to join dissimilar materials without the use of an ancillary joining method such as adhesives or fasteners.

The method presented here uses a channel cut into the metallic substrate to contain embedded polymer via an extrusion additive manufacturing process (Figure 1). Additionally, layers can then be deposited onto the embedded polymer to ultimately create a multi-material part.

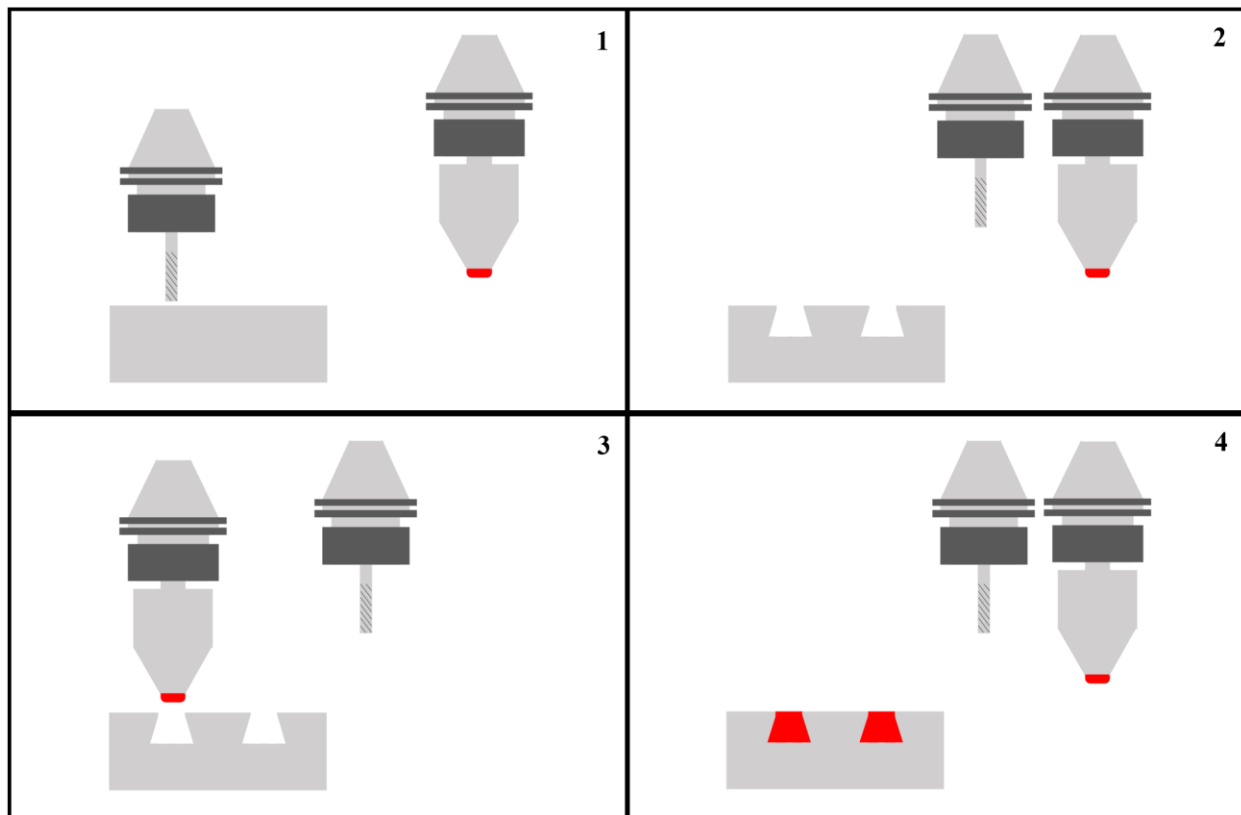


Figure 1. Process steps to embed polymer into a metallic substrate

While many different undercutting geometries can be used, it is not clear which geometry would perform best. Two experiment groups were conducted to investigate the parameter and shapes of the undercut geometry/root structures. The first experiment group developed physical testing to answer: 1) what the baseline strength of an ABS-Carbon Fiber (CF) part made using a PE-1 extruder from Hybrid Manufacturing Technologies, 2) does tensile strength of the root

structure change as the undercutting geometry changes, and 3) the effect of substrate and printing temperature on the shear strength. Using modeling, the second experiment group investigated the relationship that root structure characteristics had on the tensile and shear strength of a multi-material system. In this study, characteristics were determined to be beneficial based upon either the maximum stress withstood by the design or by the minimum displacement measured within the part.

Of the first experiment group, the initial study establishes a baseline for the strength of an additively manufactured part and identifies a printing temperature for the remaining experiments. Three forms of failure can occur: 1) failure within the part, 2) failure between the part and the root structure, and 3) failure of the root structure. It is desired that the root structure is stronger than the additively manufactured part, therefore, the tensile strength of the additively manufactured part is the baseline strength the root structure needs to exceed. The root structure should fail after the AM part because when in use, the part should not be exposed to a force that causes the part to fail. If the root structure fails before the part, the whole system fails and is designed incorrectly. Next, an investigation into the difference in tensile strength of different root structure geometries to determine if the type root structure leads to different tensile strengths was conducted. The last test of group one utilizes different printing and substrate temperatures to identify their effect on the primary bond strength. The second experiment group utilizes FEA modeling to begin to identify important characteristics that effect the strength of the root structure.

The results from the first study showed that printing temperature first positively influences tensile strength then negatively influences it, showing potential material degradation after a certain point. The results of the second study show that different root structures produce

different tensile results, but with large variation, suggesting more testing is needed. Results from the third test, show that both substrate temperature and printing temperature have a positive effect on the strength of the bond between the root structure and the part. Additionally, it shows that printing temperature had diminishing effect as the substrate temperature increases. Lastly, the FEA results begin to establish a relationship between the various characteristics of the root structure geometry and tensile strength.

1.2 Research Motivations and Problems

The motivation of this research is to add to the body of knowledge of multi-material structures produced via hybrid manufacturing. This topic is relevant to the production of multi-material structures without the use of adhesives and mechanical joints.

There are several problems that need to be addressed; 1) Does changing the print temperature affect the tensile strength of the AM part and what is the baseline strength, 2) How does the root structure affect the strength of multi-material structures, 3) How does the substrate and print temperatures affect the shear strength of a multi-material structure, and 4) What factors are most important to consider in a root structure design?

1.3 Organization

The remainder of the Thesis is organized as follows: Chapter two covers the related work across three main areas of Hybrid Manufacturing, Big Area Additive Manufacturing (BAAM), and multi-material parts. Chapter three consists of the two experiment groups run during this study and provides results and discussion. Chapter four presents conclusions from this work, discusses limitations, and outlines potential future work.

CHAPTER 2. LITERATURE REVIEW

The first section of the literature review provides a background of hybrid manufacturing, various classifications of hybrid manufacturing, and the benefit to industry. The second section presents research in Big Area Additive Manufacturing (BAAM), the classification characteristics, challenges presented with large-scale additive manufacturing, and the benefits of this manufacturing method. Finally, the third section covers an investigation of research on the use of multi-material structures in additive manufacturing methods.

2.1 Hybrid Manufacturing

Early definitions of hybrid manufacturing are limited to the work on hybrid machining as a joining of two or more material removal systems [4]. However, as systems are becoming more complex, hybrid manufacturing systems can encompass more than just subtractive systems. Other definitions take a prototype theme as they describe hybrid manufacturing as a combination of a conventional and rapid manufacturing method [5]. This research adopts the definition of “A rapid process is one that can proceed from CAD model to (process) start with little to no human interaction or skill required, typically in a short period of time” for the use of the term *rapid* in a manufacturing aspect [6]. Additionally, this research adopts the definition of hybrid manufacturing as a combination of multiple unique manufacturing processes in a new system where the unique capabilities of each unique system benefit the new system as a whole [1]. Adding multiple independent systems together creates a potential for the creation of complex part systems with improved flexibility and decreased production time [1]. Hybrid manufacturing systems have been shown to reduce manufacturing time, therefore, reducing part price while also simplifying part fixturing and reduce production planning [7]. As the demand for customization and personalization continues to rise, the design and flexibility of hybrid manufacturing systems

allows for a multitude of benefits in various industrial applications. Hybrid manufacturing has seen growth in the joint use of additive and subtractive manufacturing systems. In these systems, the AM process is used to deposit material to the correct location and then a machining process finalizes the net shape. Systems like the rapid pattern manufacturing system developed at Iowa State University simplify this method by stacking sheets of material and glue them together prior to machining [8]. Conversely, other research proposes the use of incremental manufacturing for a hybrid system. Here, parts were premade using conventional methods (i.e. casting or machining). These premade parts were then placed into an AM system where material is added in specific locations to add desired material characteristics or create complex geometry [9,10]. In this system, most of the part is created using traditional methods utilizing more cost-effective bulk material, then the desired characteristic is produced using AM.

While the ability to switch between additive and subtractive processes has shown great potential, difficulties arise in the process planning required due the differences in process planning for each individual system. CNC-RP was one of the early rapid process planning methods that brought subtractive manufacturing closer to the simplicity of additive manufacturing process planning [11]. Digital Additive Subtractive Hybrid (DASH) took the next step of development in rapid CNC process planning. Within the DASH system, machining allowances and sacrificial supports are automatically added to the users design prior to printing [12]. Next, the proposed feature-based advanced hybrid manufacturing process planning system (FAH-PS) builds from the DASH system by improving the order of operations seen in the process planning and increased the number of supported processes [13]. To gain the full benefit of multi-axis systems, some hybrid systems have utilized adaptive slicing to generate the tool path planning [14]. This allows multi-axis manufacturing to eliminate the need for support

structures when depositing material. Additionally, research can also be found on the physical production planning (what parts are being made) not only the derivation of the NC programming. Here, research focuses on the use of hybrid manufacturing to combat mass customization. This research proposes the use of product family classifications of which one base part can be mass produced and then rapidly adjusted using an AM/SM hybrid approach [15].

2.2 Big Area Additive Manufacturing

Jointly developed by the Oak Ridge National Laboratory (ORNL) and Cincinnati Inc., Big Area Additive Manufacturing (BAAM) created larger parts by using thicker layers at faster deposition rates, at the expense of surface finish using a screw extruder to deposit large amounts of pelletized polymers [16, 17]. BAAM exhibited issues with interlaminar strength, where the primary bonding between layers is a combination of thermal fusion and polymer interdiffusion, which are both dependent on the temperature of the extruded material and the previous layer [18]. Since BAAM occurs outside of a temperature-controlled environment, long layer printing times caused the plastic to cool, decreasing the interdiffusion between layers and decreasing the strength along the build direction [19]. It has been shown in smaller FDM printing that using a heated build environment and controlling the temperature of the build environment leads to increases in strength of the parts [20]. Adding fiber reinforcement, commonly carbon fiber, to the material results in increased strength in the X-Y plane of the layer while not improving strength of the Z-direction between layers [21]. The interlaminar strength has been seen to decrease by 85% when carbon fibers are added due to a reduction in contact area as a result of an increased rigidity of the bead as well as the buildup of fibers near the surface of the bead, preventing bonding [22]. While adding carbon fiber reinforcement leads to strength increases upwards of 200% in the XY plane, it also increases the dimensional accuracy significantly by reducing the CTE of the material [23]. Due to the large parts created using BAAM, a significant temperature

gradient is seen across the large part adding stress within the part. The combination of poor interlaminar strength and an increased temperature gradient lead to failures such as delamination.

To combat delamination of large parts and decreased strength, multiple solutions have been investigated. One solution looks at post-tensioning the parts by using metal tendons, similar to those seen in concrete applications, to increase the tensile strength of the parts [24]. This method requires holes to be left during printing so the metal tendons can be added and tightened after the parts have been made. Various other post processing solutions to decrease internal stress have been developed with varying levels of success. Acetone vapor has been found to improve surface finish while only marginally reducing the strength of the part [25]. The use of ionizing radiation has shown a 1.7x increase in toughness of PLA parts with potential for other materials [26]. In addition, the use of pressure and ultrasonic vibration has shown improvement in tensile properties of PLA [27]. Z-pinning, a method to leave gaps across layers to then extrude hot material across multiple layers, has been developed as an in-process solution. It has been shown to increase layer to layer strength by 10% for solid infill and 51% for a 75% dense infill when the parts are loaded in a bend test [28]. However, the results also show that problems arise when using cylindrical pins because the sample can still pull apart easily due to poor bonding between the pin and the layers adjacent. Other in-process methods use external heating to warm the previous layers prior to subsequent layer printing. Infrared preheating was used to preheat a previous layer to just above the glass transition temperature and found to significantly increase the fracture strength of samples [29]. When printing with an FDM machine, it was found that using hot air to preheat the previous layer did not provide a benefit to the interlaminar strength when loaded with a tensile force [30]. Finally, when a laser is used to create localized pre-heating, parts were found to have a 50% increase in strength [31].

2.3 Multi-material parts

Commonly, multi-material additive manufacturing has used materials from the same group classification to build parts out of two or more materials. This has been used to create composite structures that can hold either graded or distinct regions of materials created within one process/machine [32]. Currently, multi-material objects are being used in medical additive manufacturing for the use of tissue and scaffold manufacturing [22]. Others used selective laser melting (SLM) and stereolithography (SL) to create customizable dental implants with the uses of polymer and metal materials [34]. The uses of powder-based AM for metal additive manufacturing allows the alloy to be changed during printing, resulting in a customized material design for a specific purpose [35]. Powder feeders in conjunction with the use of Laser Engineered Net Shaping (LENS) can provide gradient material properties, mixing multiple powders in varying proportions. It is important to match the CTE between the dissimilar materials, control the mechanical properties, and control the alloy of the materials [36]. Other systems like stereolithography allow for the creation of multi-material structures through the mixture of different resins during the process [37]. Polyjet printing using the Stratasys Objet500 has been used to create not only multi-color parts but multi-material parts with the ability to control the thickness and rigidity of the part where it is needed [38]

Challenges using multiple materials often stems from the joining of the two materials. Differences in material characteristics such as thermal expansion, cooling rates, and melt temperature can increase stress and decrease performance [39]. Bonding also presents an issue when materials are used across material groups. Injection molding is a common process for creating multi-material plastic parts as well as metal-plastic parts. Referred to as overmolding, this process utilizes a premade part (insert), commonly metal or another polymer, that is placed into a mold where another material is added [40]. In the ideal case, the overlaid material would

be completely fused to the underlying material [41]; however, due to material differences, a bonding agent is used, or an additional process step is needed [42]. Alternatively, a mechanical interlock is used in conjunction with or in replace of a bonding agent [41]. A mechanical interlock uses an undercut geometry or reverse counterbored holes to hold the overlaid material in place, creating the only failure mechanism to be a failure of the material. Newer molding systems create hybridized parts through a process where hydroforming creates a metal insert and then injects plastic onto the part [43]. Commonly known as media based forming injection molding (MBF-IM), this process creates polymer metal hybrids (PMH) by using the same mold to form the metal component and add the plastic component in one production cycle [44].

CHAPTER 3. METHODOLOGY, RESULTS AND DISCUSSION

This section of the thesis is broken down into the two experiment groups run during this study, the results of each experiment, and discussion of the results. The first group consists of three physical laboratory tests: 1) an investigation of the tensile strength of additively manufactured parts via screw extrusion at different printing temperatures, 2) a study of tensile strength of various root structure geometry created via conventional tooling methods, and 3) samples were created to explore how substrate and print temperature affect the shear strength of multi-material structures. The second experiment group consists of theoretical models created and tested through FEA to determine what design aspects had the greatest effect on the strength of multi-material structures.

3.1 Physical Experimentation

3.1.1 Tensile Testing of AM Prints from PE-1 Extruder

(i) Methodology

The first experiment of this research consisted of traditional tensile testing, in accordance to ASTM D638 of the AM extruded plastic [45]. For this tensile test, a composite of acrylonitrile butadiene styrene (ABS) with 20% by weight chopped carbon fiber was used. This test serves as a baseline for the strength of the multi-material structures studied later.

For this experiment, the PE-1 Extruder manufactured by Hybrid Manufacturing Technologies was used within a HAAS UMC 750 milling machine (Figure 2). Using a 3mm nozzle,



Figure 2. Extruder with 3mm nozzle

sample blocks were printed at 220, 250, and 280°C (Figure 3). It is recommended that ABS be printed at temperatures between 210-270°C [46-48], and the manufacturer recommends printing at 220°C. However, it was found using a FLIR T420x infrared camera, that the plastic

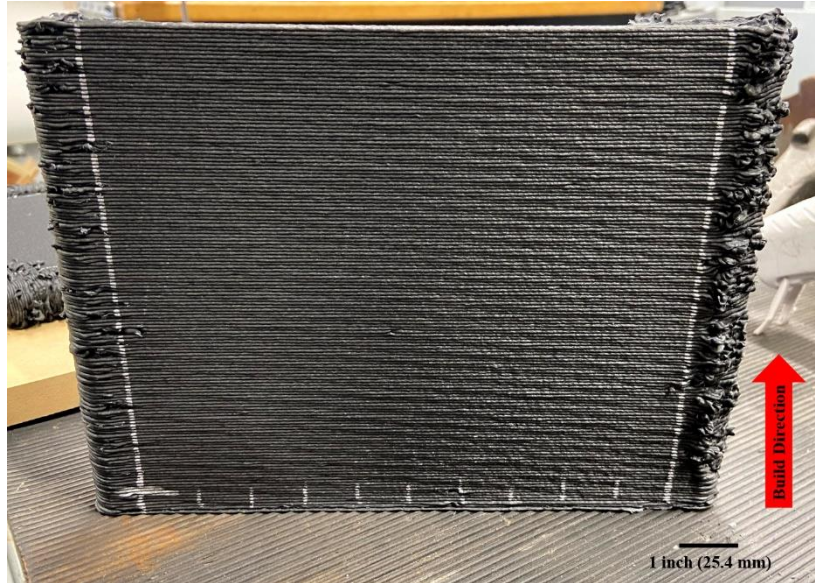


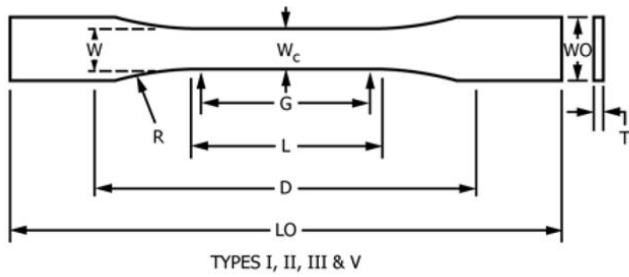
Figure 3. Material block for tensile testing

leaving the PE-1 extruder tip exhibits a temperature drop of 30-40°C from the set extruder temperature. From this discovery, temperatures of 220°C (manufacturer recommended setting), 250°C (plastic extruding at 220°C), and 280°C (30°C above 250 to have it become the median value) were chosen for this study. Table 1a provides the printing parameters used to create all three sample blocks. The Oak Ridge National Laboratory (ORNL) slicing program was used to set parameters and generate toolpaths.

Table 1. (a) Printing parameters for block creation and (b) machining parameters

Printing Parameters (a)	
Nozzle Diameter	0.12in.
Layer Height	0.05in.
Printer Base Offset	0.0in.
Minimum Table Value	0.0in.
Inset Extrusion Width	0.118in.
Infill Extrusion Width	0.118in.
Skin Extrusion Width	0.0in.
Infill Percentage	78.74%
Infill Pattern	Lines

Machining Parameters (b)	
Tool Type	3/8" Flat Endmill
Spindle Speed	1069 RPM
Feed Rate	25 in/min



Dimensions (see drawings)	7 (0.28) or under	
	Type I	Type II
W—Width of narrow section ^{E,F}	13 (0.50)	6 (0.25)
L—Length of narrow section	57 (2.25)	57 (2.25)
WO—Width overall, min ^G	19 (0.75)	19 (0.75)
WO—Width overall, min ^G
LO—Length overall, min ^H	165 (6.5)	183 (7.2)
G—Gage length ^I	50 (2.00)	50 (2.00)
G—Gage length ^I
D—Distance between grips	115 (4.5)	135 (5.3)
R—Radius of fillet	76 (3.00)	76 (3.00)
RO—Outer radius (Type IV)

Figure 4. ASTM 638-14 Dimensions for Type 1 Samples [45]

ASTM D638 Type I standard calls for a thickness of 0.28 inches (7mm) or less (Figure 4), which is just over two bead widths (bead width of 0.118 inches). To include one full bead in

the tensile bar, the block was printed 5 bead widths wide. The block was oversized in all directions; 10in. (254mm) wide, 7.25in. (184mm) tall, and 0.6in. (15mm) thick with a 0.3in. (8mm) radius on either end of the 10in. dimension. Samples were then cut with a waterjet to the rough shape;



Figure 5. Block after waterjet cutting with numbers on samples indicating location they were cut, in decreasing distance from start/stop.

print temperature and orientation identifiers were added (Figure 5 and 6).



Figure 6. Tensile bar prior to machining in (a) isometric (b) top and (c) left side view

Next, the first machining process machined halfway through the first bead on the front (arrow indication) and profiled the final geometry of the bar. The part was then flipped over, and the second machining process milled off the remaining material to create the desired thickness of 0.28 inches (7mm) or less, resulting in a finished part (Figure 7). Eight samples were made for each print temperature.



Figure 7. (a) Finalized tensile samples and (b) samples during testing

Thickness and width measurements were then taken at the center of the neck region and at locations ± 25 mm from the center to calculate the stress after testing. Testing occurred after the samples were conditioned in accordance to ASTM D638-14 with a Testing Resources 800LE2 testing machine (Figure 7b). Testing showed that applying a load at a rate of 0.2in./min created failure prior to the 0.5-minute mark. Therefore, the load was applied at a rate of 0.01in./min for failure occurring after the 0.5-minute mark and prior to 5 minutes; results of this experiment are presented in the following section.

(ii) Results

Samples that broke outside of the necking region were discarded; $n = 7$ samples for 220°C and $n = 5$ for the sets printed at 250 and 280°C. No conclusions were made on the locations of each break due to lack of control of orientation (top versus bottom of the block) during testing. From visual inspection, all observed breaks seemed to occur between layers, which was expected (Figure 8). Breaks that occurred outside the necking region included printing defects (voids, cracks, or other form of layer defects). It is hypothesized that these printing defects caused those samples to break outside the necking region.

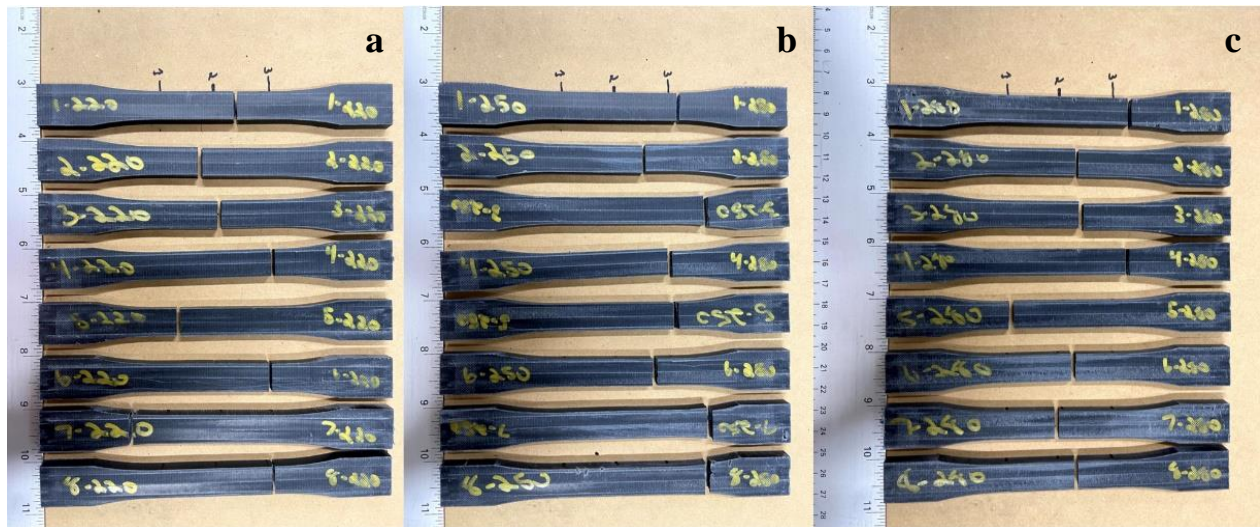


Figure 8. Tensile bar samples at (a) 220°C, (b) 250°C, and (c) 280°C

Mean samples were calculated with a $\pm 95\%$ confidence interval (Figure 9). Although conclusions could not be made as to which temperature is optimal, several observations can be

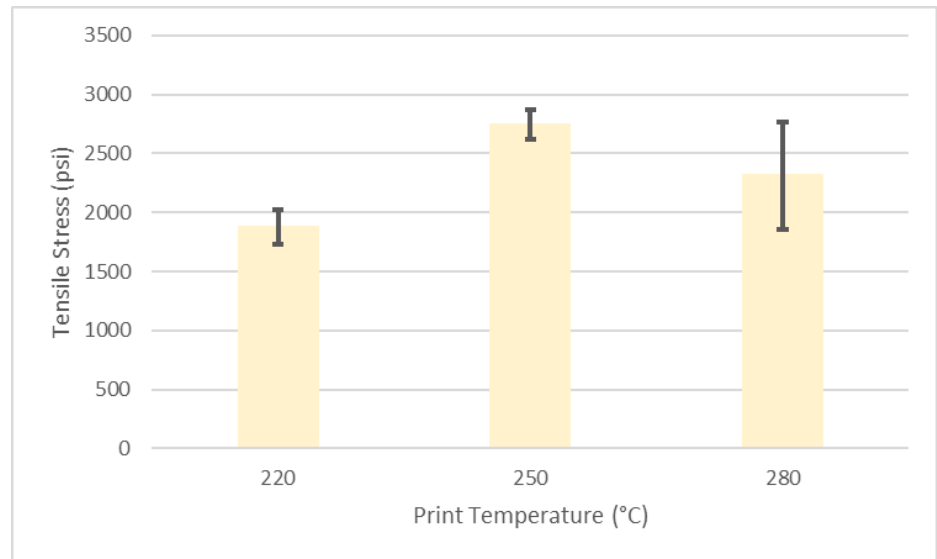


Figure 9. Mean tensile stress

made. Both the 220°C and 250°C group have small standard deviations (160 and 101psi respectively) and therefore, small confidence intervals. Figure 9 shows statistical evidence that printing at 250°C leads to parts with a higher tensile strength than at 220°C, with mean values of 2,746psi versus 1,876psi. However, the mean values of both the 220°C and 250°C do not differ statistically from the 280°C parts. The standard deviation for the 280°C parts (364psi) is approximately 2.3 and 3.6 times larger than standard deviations of the 220°C and 250°C parts, respectively. That suggests there is more variation in the 280°C printed parts, potentially from material degradation at higher printing temperatures. Therefore, there is no evidence to suggest that printing at 280°C provides any benefit over the other two printing temperatures.

One potential outlier, 1,678psi, is seen in the 280°C sample group and is vastly smaller than the other four samples (range from 2,385-2,566psi). When removed, the standard deviation of the sample group decreased from 364psi to 95psi. The mean strength of the sample group increases from 2,312psi to 2,471psi. This outlier is most likely a product of this manufacturing process due to the variability seen in an additive manufacturing process. When this outlier is

removed, the parts printed at 280°C now have a statistically higher strength from the 220°C prints (Figure 10). The confidence intervals for the 250°C prints (2,620psi lower limit) and the 280°C prints (2,622psi upper limit) still overlap and by definition, the 250°C and 280°C parts are

not statistically different. However, this overlap is so small that further experimentation is probably warranted. One can observe a trend that there is

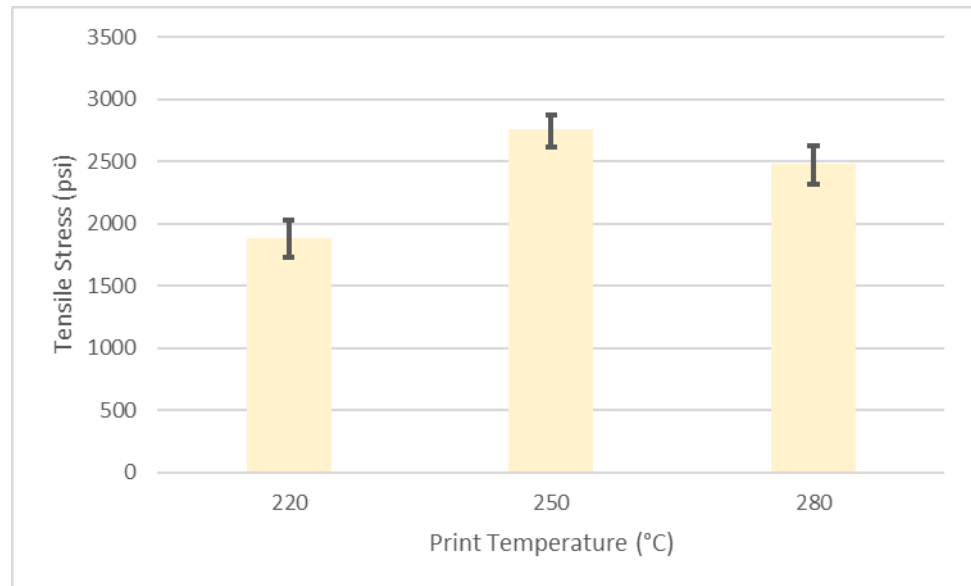


Figure 10. Mean tensile stress with the removal outlier

an increase in strength from 220°C to 250°C and a decrease in strength from 250°C to 280°C. This may suggest that degradation of the plastic occurs when printing over 250°C. In air, the degradation onset temperature (DOT) of ABS is 310°C, which is the temperature at which 1% weight loss is observed in the thermogravimetric analysis (TGA) [49]. This could be to the internal temperature of the screw extruder being at 30-40°C higher than 280°C. Therefore, printing at temperatures higher than 250°C with this extruder and material may not be beneficial. Regardless, the results from this study suggested the use of 250°C for the next physical tests.

3.1.2 Tensile Testing of Root Structure Design

(i) Methodology

The focus of the next section is an investigation of root structure geometry. For this study, the substrate material was 6061 aluminum bar stock and the AM material remained the same as ABS-CF (20 wt.%). Due to the difference in strength between the two materials, the

baseline for the strength of the multi-material structure is assumed to be the weaker tensile strength of the additively manufactured ABS-CF.

Five different root structure geometries were investigated; the root structure profile was the same for all, a rectangular closed circuit (Figure 11a). The substrate was held at 2in.x2in.x0.5in (51mmx51mmx13mm) for all samples. The profile of the root structure was a centered 1in.x1in. (25.4mmx25.4mm) square on the substrate. All the geometries were machined using conventional tool geometries (Figure 11b-f). The geometries included the following: 1/4in. 20° Dovetail (Harvey Tool – 877416), 1/4in. 40° Dovetail (Harvey Tool – 864016), 1/8in. 270° Undercutting End Mill/Lollipop (Harvey Tool – 41308), 1/4in. Keyseat Cutter/T-slot (Harvey Tool – 43962), and a 1/4in. 18-56 TPI Thread Mill (MSC Direct – 57568834). When printing

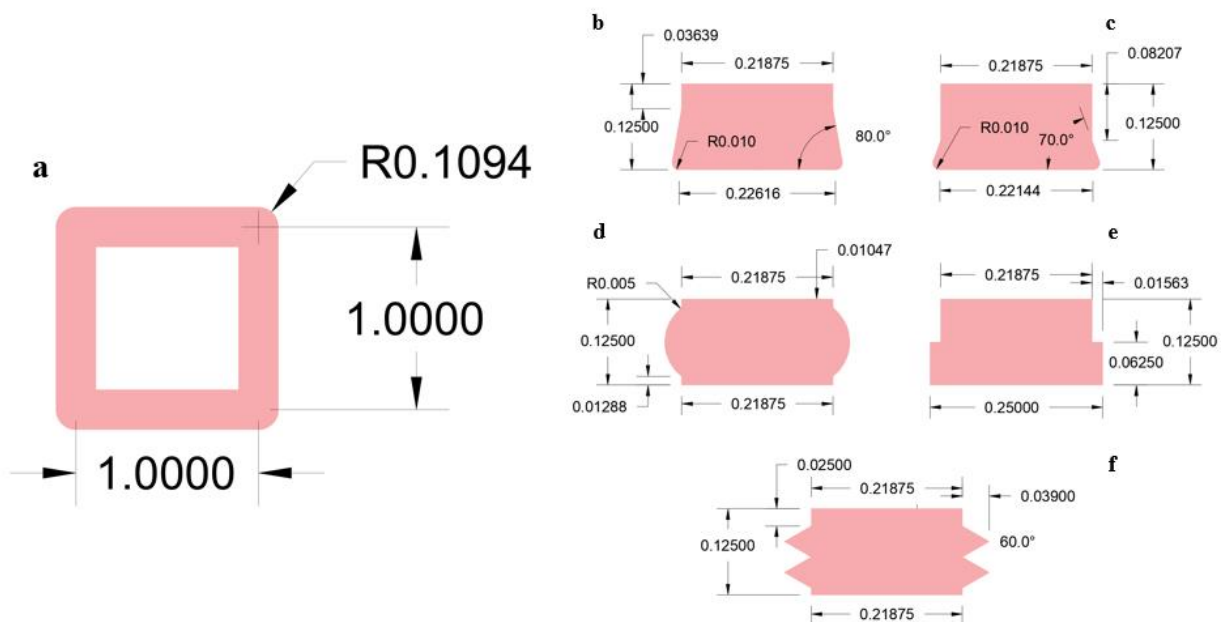


Figure 11. Root structure profile (a) and root cross sections; (b) 20° Dovetail, (c) 40° Dovetail, (d) Lollipop, (e) T-slot, (f) Threaded (inches)

onto a metallic substrate, it was discovered that the fixation of the plastic into the roots was improved when a closed loop is used versus an open ended slot [50]. It is hypothesized that when the extruded material cools, that the natural contraction of the material creates a clamping effect

onto the substrate into which it is deposited and the closed loop accounts for shrinkage in all directions [50]. Although more complex profiles may perform better, for simplicity and repeatability of this experiment, a simple square profile was used.

All the samples started with the same first two machining steps: 1) a 1/4in. clearance hole was drilled to a depth of 1/8in. (tip compensation on), and 2) a 7/32in. flat end mill (2 flute) was used to rough out the channel to the final depth of 1/8in. The width of the channel at the top (7/32") and the depth of the channel (1/8") remained constant. The geometry on the faces perpendicular to the surface of the substrate was milled depending upon the sample design. It should be noted that the threads were not designed with a traditional spiral seen in threads, but rather stacked triangular grooves. This configuration will be referred to as "threads" for the remainder of this thesis. To accommodate the change in volume of the channels, the plastic was over extruded at 250°C into the channels. Cross-sections of each different root structure geometry and the over extrusion of plastic are presented in Figure 12. The plastic was machined to 0.05in. (1mm) above the substrate to provide isolation of the root structure and to avoid creep.

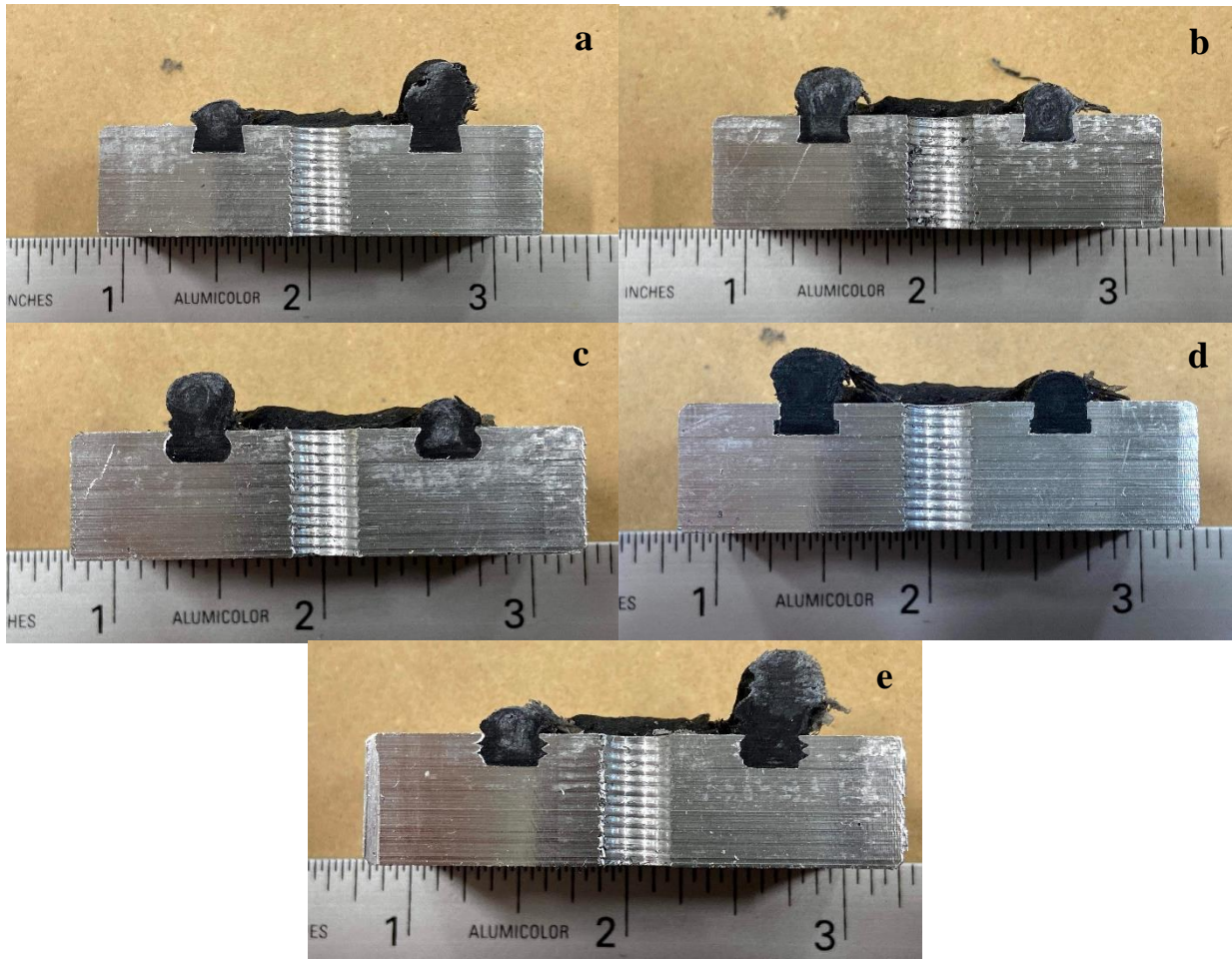


Figure 12. Cross section of (a) 20° Dovetail, (b) 40° Dovetail, (c) Lollipop, (d) T-slot, (e) Threaded root structure geometries

While no testing method exists for the proposed joining method, an adaptation of ASTM D897-08 was chosen. In this testing method, a block of ABS was adhered to the top of the plastic root structure (Figure 13). A 5/16"-24 rod end was then screwed into each block to allow for four degrees of freedom during the tensile test in accordance with ASTM D897-08. The adhesion

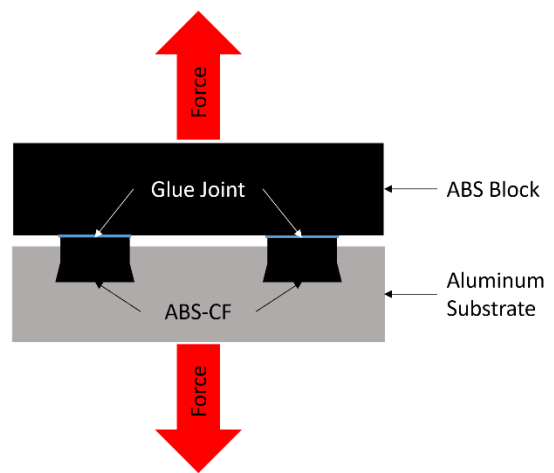


Figure 13. Sample testing setup

between the top block and the root structure was achieved using solvent welding with 100% acetone.

Both the block and the root structure were lightly sanded with 80 grit sandpaper, wiped clean using 70% isopropyl alcohol, and then 0.8cc of 100% acetone was added to the surface of the ABS block (Figure 14a). The root structure and aluminum were then immediately placed on top of the block to adhere the plastics together. To maintain a constant clamping force across all samples, a 5/16in.-24 bolt and washer was passed through the ABS block and screwed into the aluminum substrate (Figure 14b), with the bolt torqued down using the same max drill clutch setting for all samples.

Due to the weaker strength of the ABS block, the rod end could not be threaded into the ABS. Another block of 6061 aluminum (2in.x2in.x0.05in.) was added to the

ABS block, joined by four countersunk bolts with a washer and two nuts on each bolt to distribute the load and prevent loosening of the threads (Figure 15). Ten samples were created for each root structure geometry in accordance of ASTM D897-08. Samples were loaded into a Shimadzu UH-300 testing frame and loaded at a rate of 0.01in./min (Figure 16). Each failure load was recorded, and the cross-sectional area of each unique geometry was calculated to determine the stress applied.

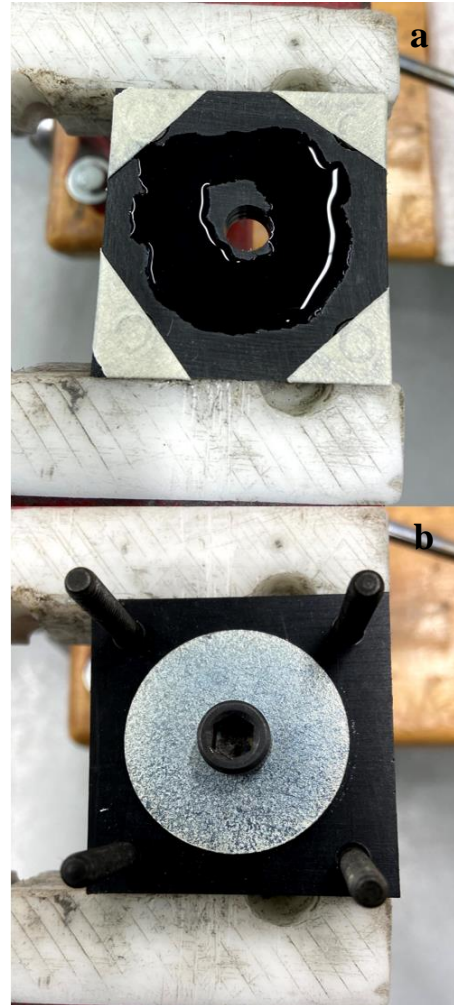


Figure 14. (a) Application of acetone, (b) bolting of the assembly

(ii) Results

During testing, two failure modes were seen: 1) failure of the root and 2) failure of the solvent weld. For failure mode 1, the stress calculation was completed by taking the force of the sample failure and dividing it by the engineered cross-sectional area of the root structure geometry (Table 4). If failure mode 2 occurred, determination was made to keep or remove the sample based upon the observations during testing.

For the 20° Dovetail samples, one sample failed at the solvent weld. Since only three of the four bolts holding the plastic block to the aluminum block were tightened the sample was removed, resulting in $n = 9$ samples. All the 40° Dovetail samples failed via root structure failure; therefore, the sample size remains at $n = 10$. Upon visual inspection, both types of dovetail root structures experienced the same failure method; shear and deformation of the root structure (Figure 17). The plastic in the undercut region began to shear and deform underneath the main structure of the channel (rectangular portion). While the 40° dovetail only has a 2.6% reduction in cross-sectional area from the 20° dovetail, it experiences just



Figure 15. Aluminum block bolted to ABS block (Note: all tested samples had two nuts per bolt)

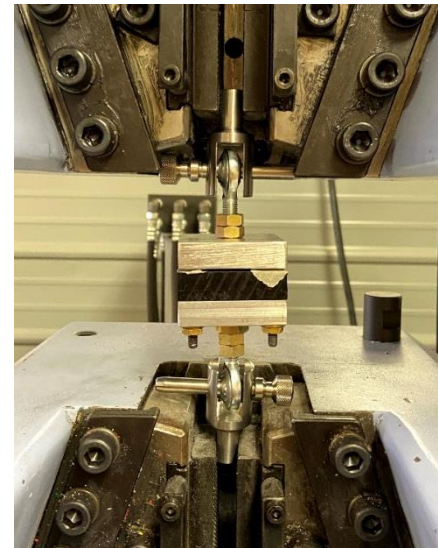


Figure 16. Root structure geometry tensile test

Table 2. Root structure cross-section area

Root Structure Geometry	Cross-sectional Area (in ²)
20° Dovetail	0.02866089
40° Dovetail	0.02791554
Lollipop	0.03071794
T-slot	0.02929688
Thread	0.0307871

under a 47% decrease in mean stress (Table 3). Increasing the undercut area appears to increase the resistance to deformation. The 20° dovetail samples had evidence of more shearing of the plastic while the 40° dovetail samples had more evidence of displacement of the plastic.

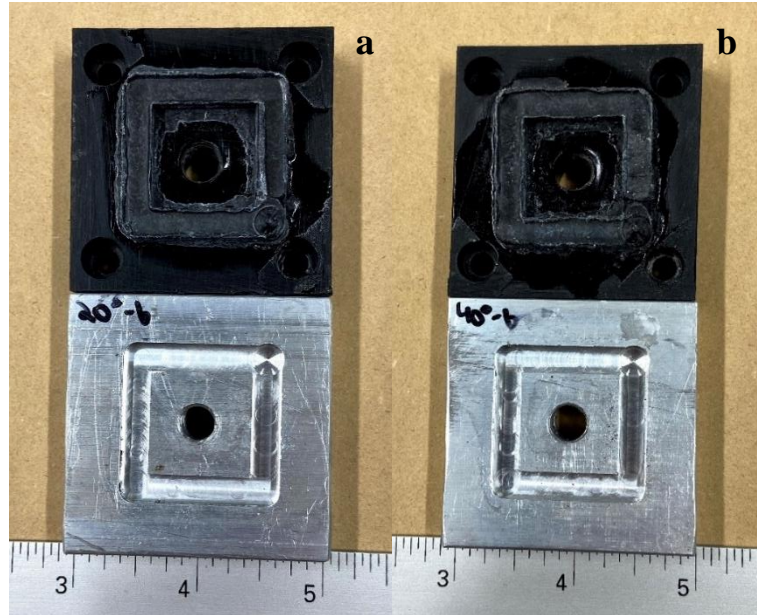


Figure 17. (a) 20° dovetail and (b) 40° dovetail

Of the ten lollipop samples, two samples failed due to failure of the solvent weld. The samples failed at 1,230lbf and 1,327lbf, the highest forces out of all 50 samples. Because both

Table 3. Mean stress results

Root Structure	Mean Stress (psi)	Std Dev (psi)
20° Dovetail	21,126	7,516
40° Dovetail	11,199	2,058
Lollipop	29,959	7,380
T-Slot	23,584	5,041
Thread	26,087	5,223

samples failed at such high forces, it is difficult to say if they were outliers of this study. The force of both samples was 19-25% greater than the next highest sample, which was in a different sample group (Thread sample: 996lbf), therefore, these samples remain in the data collected and $n = 10$ samples for this data set. Of the remaining two root structure geometries, the t-slot samples all failed via root structure failure: $n = 10$ samples. One thread sample failed due to the weld failing at 921lbf, within the range of failure forces seen with the thread samples (637-995lbf). Therefore, this sample is removed from the sample group due to the failure not occurring in the same way as all the other samples in this sample group and $n = 9$ samples.

The lollipop and the thread designs failed in similar fashion; via a ripping/shearing of the undercut plastic from the plastic of the main channel (Figure 18). Both the lollipop and the

thread root structures had the top performing mean stresses out of all five designs (Table 3). The t-slot design, the third highest performer (Table 3), had a failure mode somewhere between

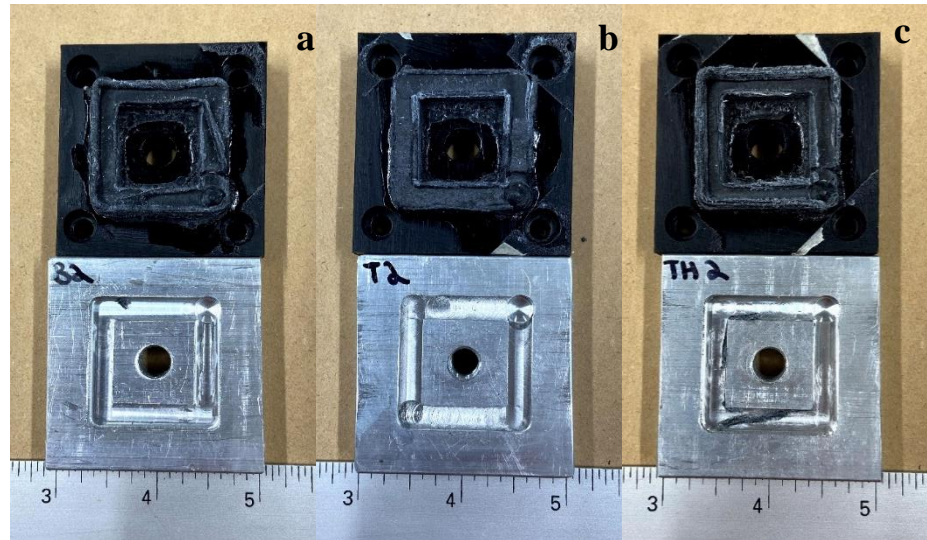


Figure 18. Failure modes of (a) Lollipop, (b) T-slot, and (c) Thread root structure design

that seen of the dovetail designs and the lollipop/thread designs. These three samples have the three largest cross-sectional area (lollipop-largest, t-slot-third largest) and experience displacement of the undercut plastic in some areas and shearing of the plastic in other areas. The flat surfaces on the bottom side of the undercut geometry in the dovetail and t-slot designs may then allow for plastic deformation prior to shearing of the material. This ability to displace the material rather than shearing it may decrease the overall strength of the root structure geometry.

Mean values suggest the lollipop design as the optimal geometry, however, the 95% confidence intervals present less evidence (Figure 19). From the confidence interval, the 40° dovetail is the only root structure that is statistically different and is statistically worse than the other four designs. The large variation seen in the other four root structure designs presents a large amount of statistical uncertainty. Variation is common in AM parts and makes it difficult to say if there is a difference between the 20° dovetail, lollipop, t-slot, and thread root structure

geometry. Mean values suggest the lollipop design performs better than other designs, but a conclusion cannot be made on which root structure geometry is optimal. However,

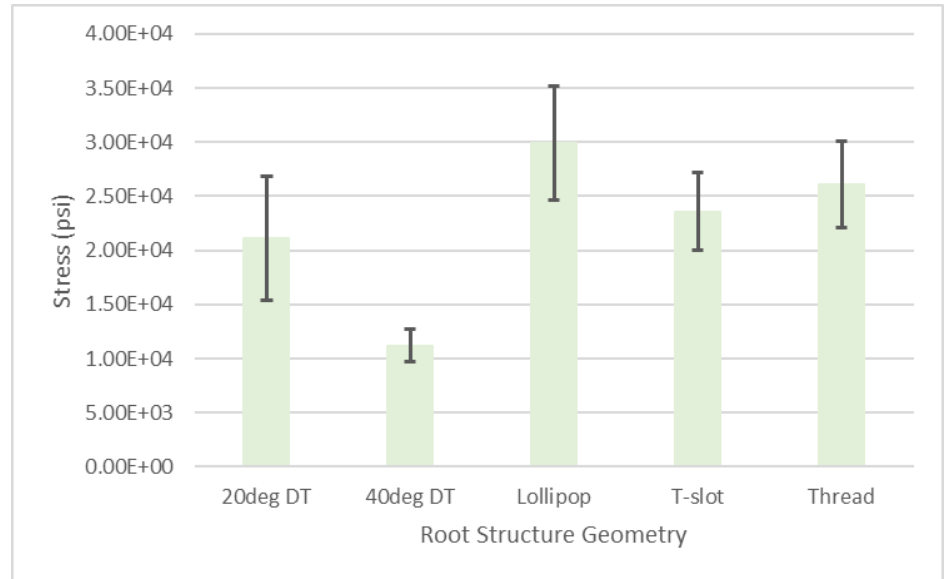


Figure 19. Mean tensile stress

the 40° dovetail performs the worst out of all five designs. From experiment one, a baseline of 2,746psi was established for delamination failure. All root structures failed due to the ABS-CF material yielding, not delamination between layers. When comparing to the delamination stress, all root structures performed better (4-11x) than the baseline stress seen in experiment one. Therefore, in a part made via this hybrid method, the AM part will experience a delamination failure prior to the root structure failing.

3.1.3 Shear Tests Across Printing and Substrate Temperatures

(i) Methodology

This experiment investigates the effects of print and substrate temperature on the shear strength of the primary bond between the root structure (layer 0) and the first print layer (layer 1) (Figure 20). Early laboratory tests showed that pre-heating the substrate leads to an increase in bond strength between layer 0 and layer 1 [50]. The plastic cools very rapidly because of the high thermal conductivity of aluminum inhibiting crosslinking between layer 0 and layer 1. Three ways to combat this challenge include: change the substrate, increase the print temperature, or increase the substrate temperature. This experiment looks at the latter two

options. For this experiment, the materials remained the same as the previous experiment, but the substrate size was adjusted to

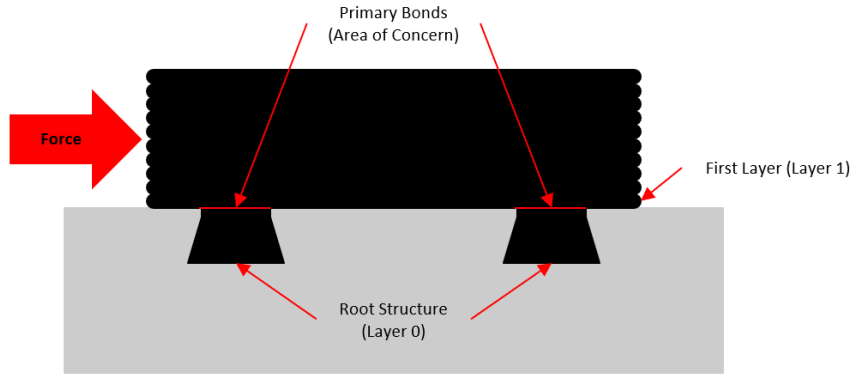


Figure 20. Schematic of primary bond as the area of concern

2.5in.x2in.x0.5in. (64mmx51mmx13mm) to accommodate for the shear testing method. A 20° dovetail was used while root structure profile remained the same square shape as the previous experiment (Figure 8).

Printing and substrate temperatures can be seen in Table 4 along with the spindle speed and feed rate of the printing process in Table 5. All other variables remain constant. Prior to printing, each aluminum substrate was preheated on a hotplate to bring it to the desired temperature. Substrates at 20°C (room temperature) were left out for 24 hours to ensure that they remained at room temperature. An insertion heater in an aluminum block was used to hold the substrate temperature while printing. Surface temperature was verified with a

Table 5. Experiment Design

	Print Temperature	Substrate Temperature
Low Level	220C	20C
Medium Level	250C	60C
High Level	280C	100C

Table 4. Dimensions and parameters of shear block samples

Plastic Block	1.125in.x1.125in.x0.5in.
Aluminum Substrate	2.5in.x2in.x0.5in
Root Profile	1in.x1in. Centered Square
Root Depth	1/8in.
Top of Root Width	7/32in.
Root Structure Geometry	20° Dovetail

	Spindle Speed (RPM)	Feed Rate (in/min)
Root Print	18	13.5
Block Print	25	59.1

thermocouple before printing. Substrates were reheated or cooled with compressed air if the desired temperature was not attained. A plastic block was printed on top of the root structure immediately following the completion of the root structure print (Table 5). Printing temperature remained constant for the root structure and block but the spindle speed and the feed rate (travel speed) were increased (Table 5).

Three print temperatures of 220°C, 250°C, and 280°C were used across three different substrate temperatures of 20°C, 60°C, and 100°C (Table 4). For this study, 100°C was chosen since the glass transition temperature (T_g) of ABS is between 94-110°C and the limitations of the insertion heater [18, 29, 49]. T_g is the critical point for diffusion across the interface resulting in improved strength [29]. Time limitations prevented testing past T_g . 60°C was chosen because it is the halfway point between room temperature and the glass transition temperature. For each print temperature, five samples were created at each substrate temperature due to time limitations. Prior to testing, the printed block's sides were profile milled to ensure a perpendicular face between the top of the substrate and the side of the block (Figure 21). All samples were allowed to cool prior to machining.

Testing methods were adapted to investigate the quality of these parts. Khorasani developed a method for testing the bond between a block created via Direct

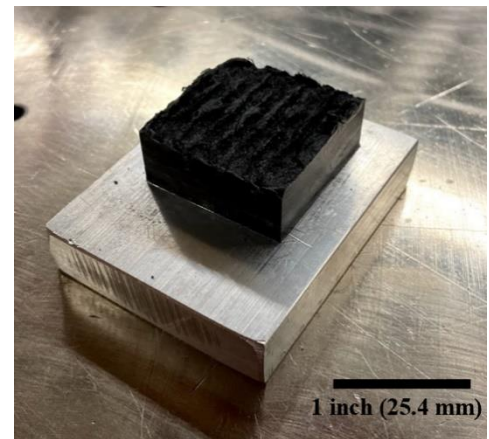


Figure 21. Shear test sample prior to testing, size in Table 4 above

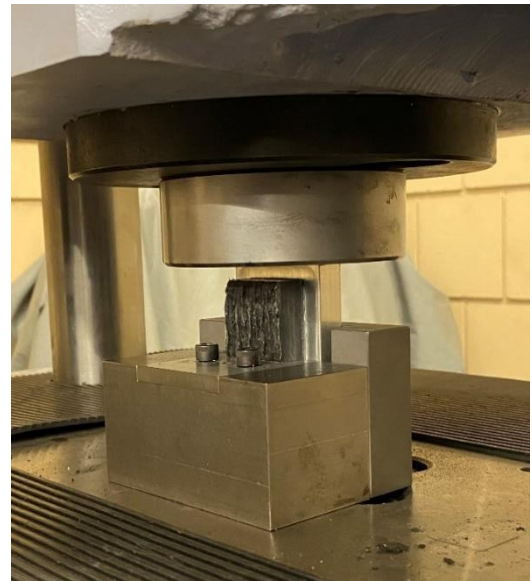


Figure 22. Block shear test

Energy Deposition (DED) additive manufacturing and the substrate it is printed on [51]. This testing method was adapted to test the interlaminar strength of the primary bond, focusing on the primary bond. Samples were loaded into a Shimadzu UH-300 testing frame and loaded at a rate of 0.01in./min, calculating stress using the maximum force divided by the area of the root profile (Figure 11a). All samples were left at room temperature for at least 24 hours prior to testing.

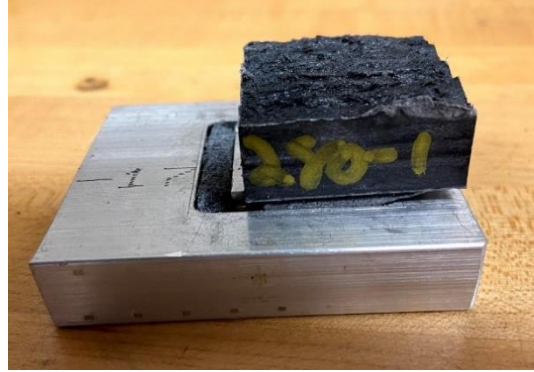


Figure 23. Broken shear sample

(ii) Results

For this experiment, all samples were successfully broken, and all samples had the same failure mode (Figure 23). Each sample group is compared using the calculated mean value and a $\pm 95\%$ confidence interval. Color groups represent print temperature with substrate temperature increasing from left to right (Figure 24)

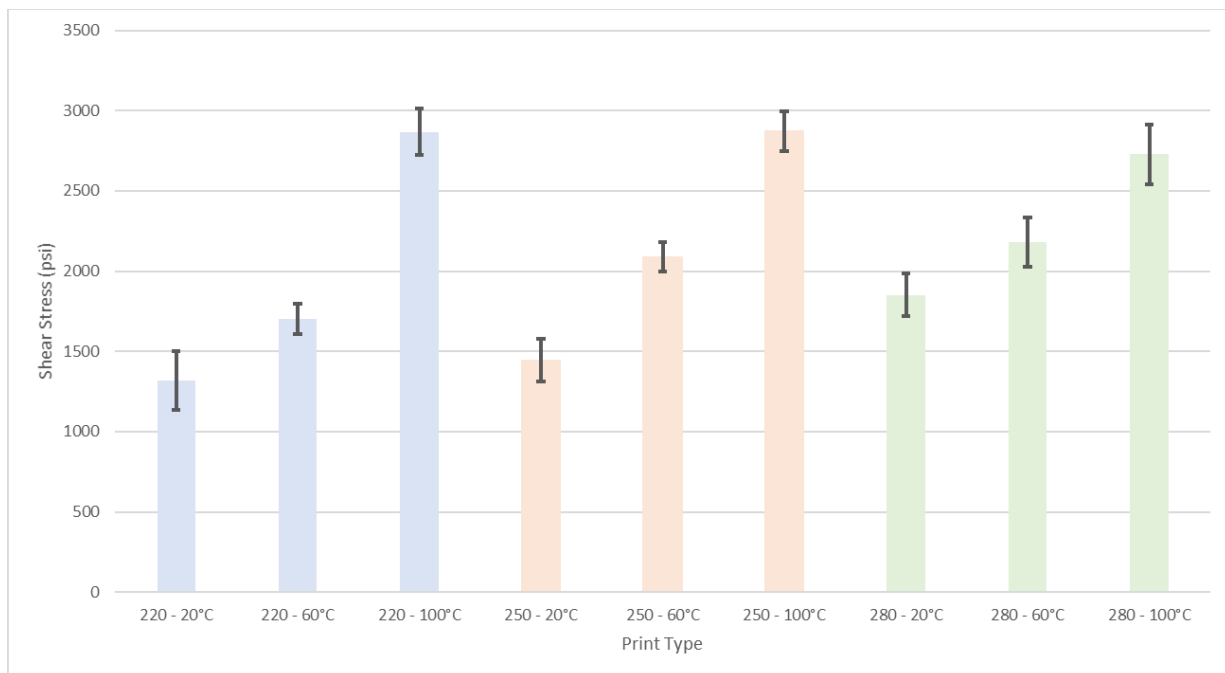


Figure 24. Mean shear stress

As printing temperature is held constant, each increase in substrate temperature leads to a statistically significant increase in the mean shear stress. Holding the substrate temperature at 20°C, there is evidence that the mean value for printing at 220°C and 250°C are not statistically different (1,317psi and 1,444psi respectively). It also shows that printing at 280°C has a statistically higher shear strength, 1,852psi. As the aluminum rapidly cools the plastic root, increasing the printing temperature increases the time the root is above T_g (open time). The increased open time provides more time for the next layer to be printed improving bond strength. When the substrate is held at 60°C, the shear stress across all printing temperatures increases. Increasing the substrate temperature leads to an increase in the open time of each printing temperature. As the substrate temperature is held at 60°C, there is no longer a statistical difference between the mean shear stress of the 250°C and 280°C samples (2,088psi and 2,198psi respectively). There is a statistical increase in the 220°C samples when the substrate temperature increases to 60°C, the mean shear strength of 1,702psi is still statistically lower than those printed at 250°C and 280°C. Lastly, when the substrate is heated to 100°C, all sample means increase at each print temperature (2,867psi at 220°C, 2,871psi at 250°C, and 2,728psi at 280°C). When that happens, there is no longer a statistical difference between the three print temperatures. As substrate temperature increases, printing temperature has a decreasing effect as the substrate temperature approaches the glass transition temperature. More experimentation is needed to conclude about alternate materials or increased substrate mass.

3.2 Theoretical Modeling

While the second experiment investigated different types of root structure's effect on tensile stress, the following FEA experiment studies the geometric characteristics of the root geometry and its effect on interface strength. This study is broken into three subsections covering Dovetail, Lollipop, and Thread Designs.

The simulation tool in SolidWorks 2018 was used for FEA modeling. This analysis uses the same part design and materials as in section 3.1.2. SolidWorks 2018 did not have an ABS-CF composite so it was decided that the non-composite ABS material would be adequate for comparison. The experiments study the effect of the root geometry on stress, therefore, direct comparisons between this experiment and the previous experiments should not be made. All models were simplified into a 2D cross-section of the part (Figure 35). Due to the simulation taking place over multiple days, care was taken to ensure that all the simulation parameters were held constant during the testing, specifically the meshing of the parts. Simulations were run to either maximum displacement (root structure pulls out of the channel) or either one of the materials fails. Figure 25 shows that two identical and parallel root structures were used; the subsequent figures only show the geometry of one of the roots.

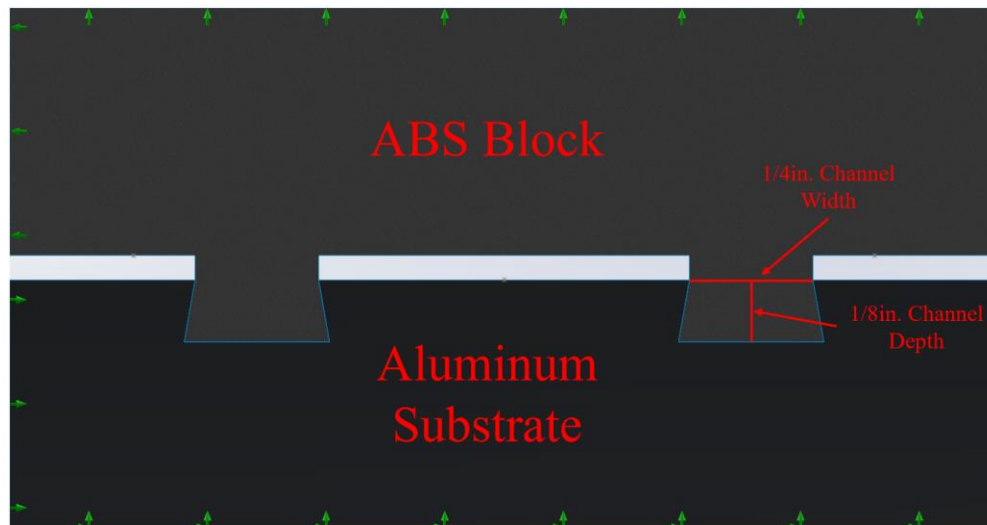


Figure 25. 2D cross-section of FEA model

3.2.1 Dovetail Design

1a Methodology – Included Angle

The primary study considered how the stress of each part varied as the included angle of the dovetail changed. For this study, an included angle of 10° to 130° was explored in 10°

increments. A dovetail of 0° included angle is simply a straight walled slot and was omitted. For this test, the width of the top of the channel ($1/4$ in.) and the depth of the channel ($1/8$ in.) remained constant. The sides of the channel changed as the included angle changed (Figure 26). The sides were coincident with the corners of the channel. This same test was run two more times by offsetting the intersection point of the sidewalls below the surface of the substrate by $1/32$ in. for the first variation and $1/16$ in. for the second variation (Figure 27). The

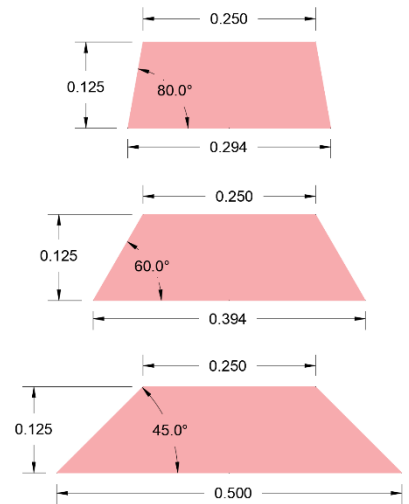


Figure 26. Schematic of change in included angle

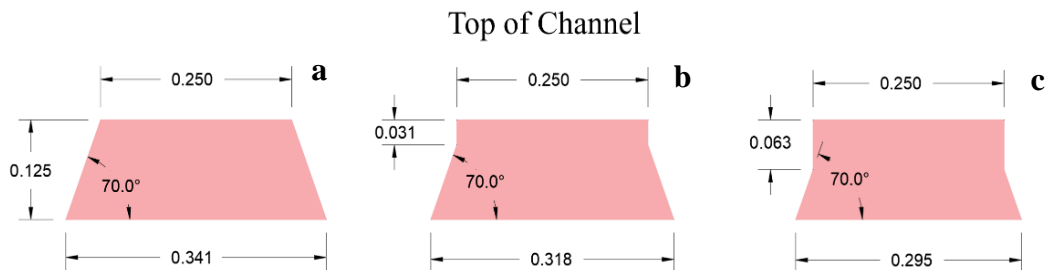


Figure 27. Schematic of (a) 0in. offset, (b) $1/32$ in. offset, and (c) $1/16$ in. offset bottom of the channel was kept $1/8$ in. from the top of the aluminum substrate.

1b Results – Included Angle

Figure 28 presents the change in included angle. All three sample types between 10 - 80° dovetails follow an increasing linear trend of maximum stress. The maximum stress was achieved with the 80° dovetail with no offset from the top of the substrate. After 80° , the benefit of increasing the included angle of the dovetail diminishes, similarly for when the offset of the dovetail is $1/16$ in. The results for the $1/32$ in offset follow a similar trend but have a shifted peak, where the maximum stress was achieved at 70° .

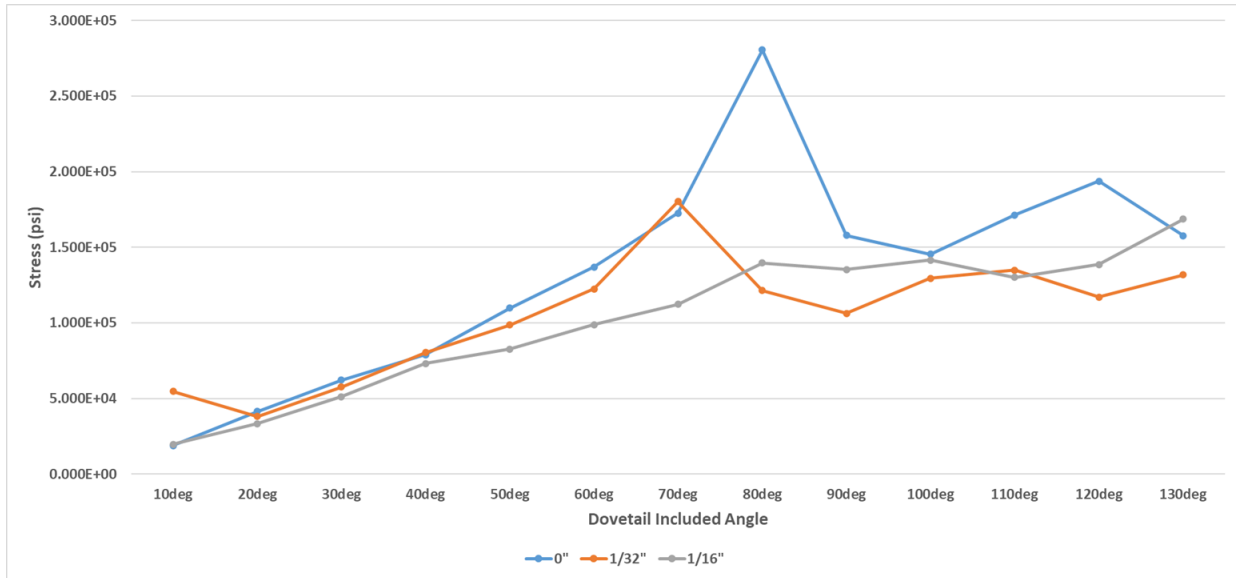


Figure 28. Maximum stress vs. included angle

2a Methodology – Depth Change

Next, simulations were run to investigate the effect of depth of the root structure on the maximum stress. The shape was held constant; 1/4in. top width, 1/8in. depth, sides remained constant based upon the dovetail being tested (Figure 29). The dovetail geometry was offset from the top of the aluminum at increments of 0in., 1/32in., 1/16in., 1/8in., and 1/4in. Additionally, a shear force was also tested. While the geometry and the depths of the root structure remained constant, the offset between the plastic block and the aluminum substrate was eliminated (Figure 30).

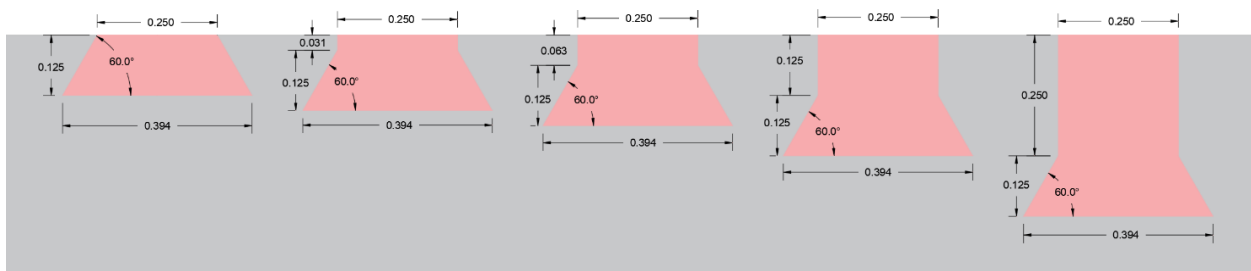


Figure 29. Schematic of change in depth

2b Results – Depth Change

Based upon results of the previous experiment, samples were only taken at 20°, 40°, 60°, 80°, and 100° for the remainder of this section. From the plots of the tensile testing at different depths and different dovetail angles, the data is inconclusive (Figure 31). In this

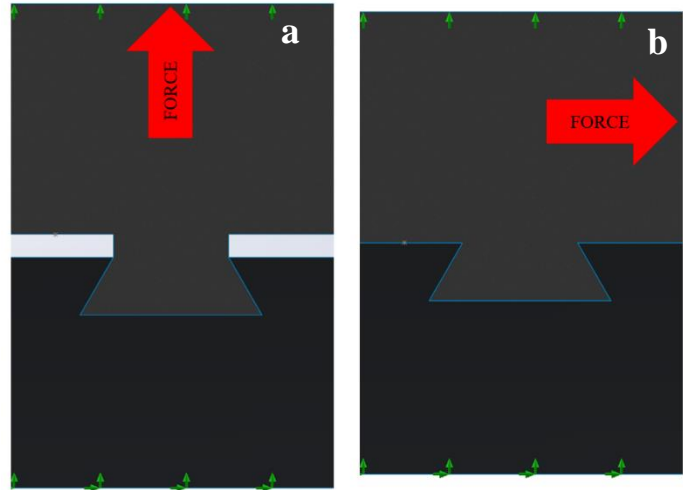


Figure 30. (a) tensile test vs. (b) shear test

study, an increase in the tensile stress would indicate an improvement within the system design; however, the results are variable for each data set.

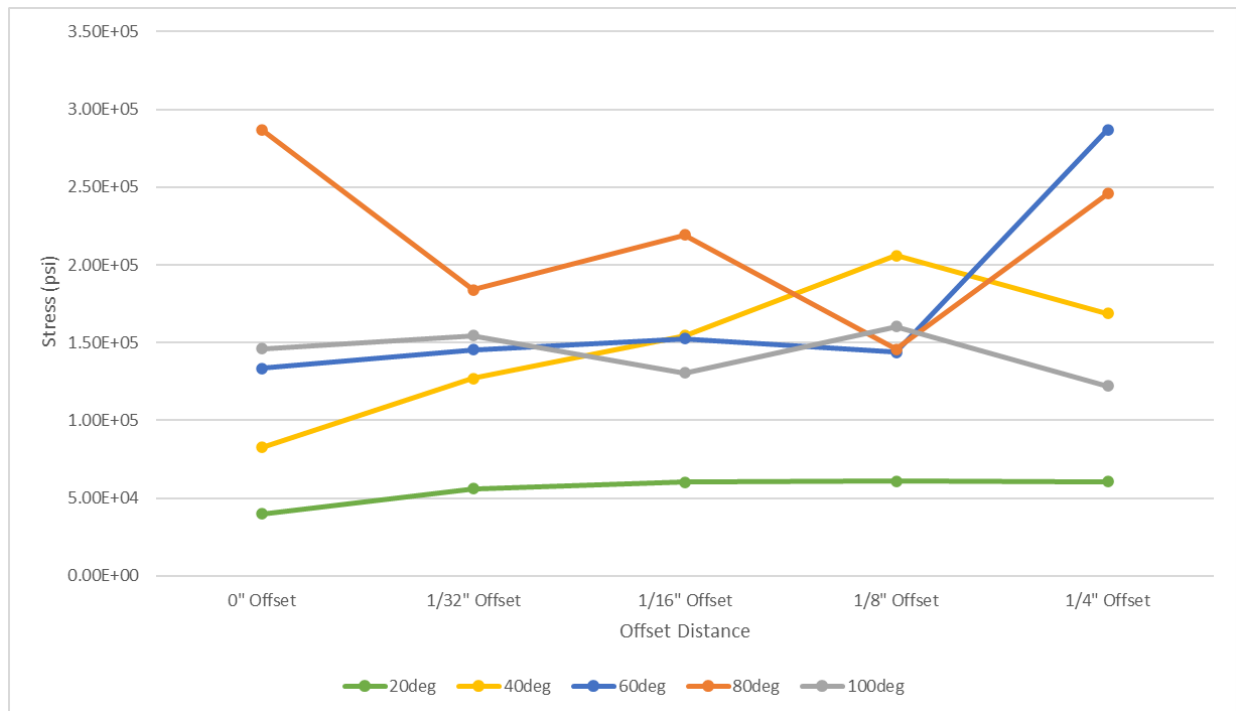


Figure 31. Tensile stress as depth of the root structure changes

For the 20° dovetail, a negligible increase in tensile stress is seen as the depth of the root structure increases. The 60° dovetail follows a similar trend as the 20° dovetail, but the stress seen when the root structure is 1/4in. deep into the substrate seems to be an outlier. The 100°

dovetail shows no effect of the depth of the root structure on the tensile strength. The 40° sample set shows the only positively increasing trend. This result suggests that when using a 40° dovetail, results improve as depth increases. The data from the 80° sample set provides the most inconclusive evidence. Overall, there seems to be a decreasing trend of tensile stress as the depth of the root structure increases and inconclusive evidence overall.

When loading this system with a shear force, it logically makes sense to not have the side wall of the channel and the top of the substrate come together at a sharp point to decrease stress concentration. From a design aspect, it would make sense to put an offset between the top of the substrate and the root structure geometry (dovetail). There does not seem to be evidence, from a tensile stress aspect, against implementing an offset from the top of the substrate into the root structure.

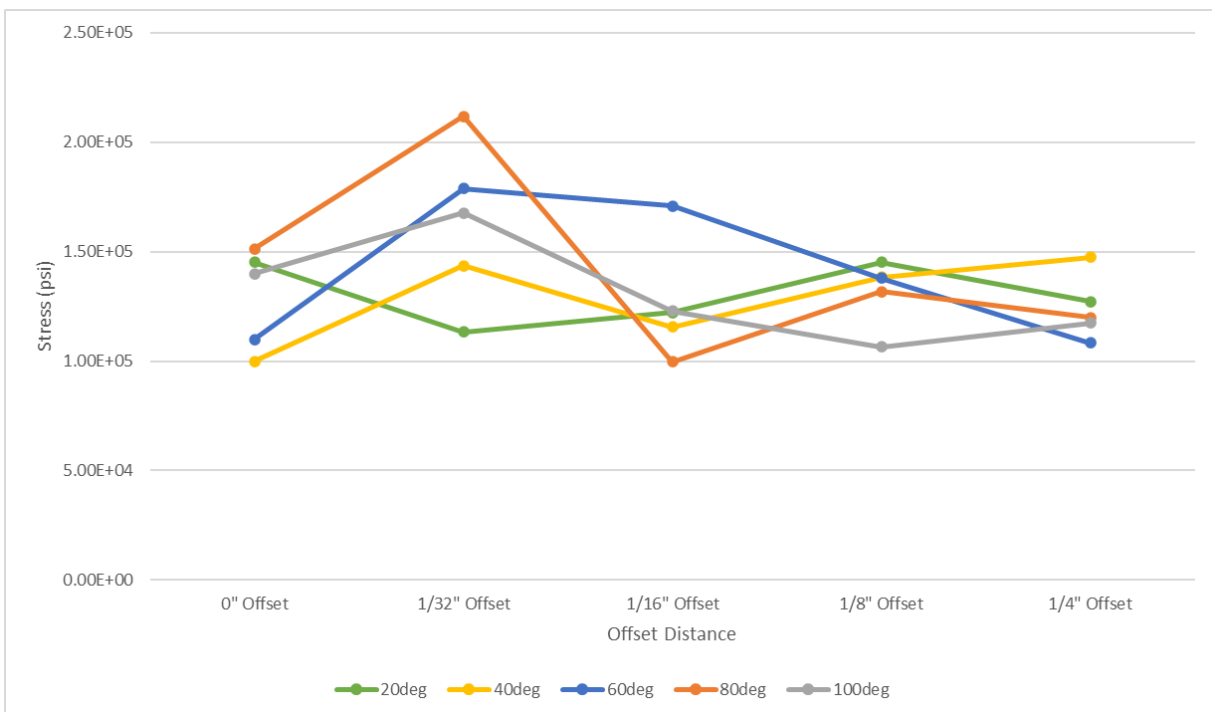


Figure 32. Shear stress as depth of the root structure changes

Offsetting the root structure geometry 1/32in. leads to an increase in the shear strength of all models except for the 20° dovetail (Figure 32). Excluding the 20° dovetail, all other sample

groups have diminishing returns as the depth of the root structure increases past 1/32in. towards 1/4in. From the characteristics of the plot above, it is hypothesized that as the root structure geometry descends below a depth of 1/4in. it has a diminishing effect on the overall shear strength of the part. From a design perspective, offsetting the root structure geometry has two main advantages. First, it decreases the sharp point that occurs at the top of the channel, decreasing the stress concentration and improving the ultimate shear strength of the system. And second, adding the offset adds more of the substrate material above the root structure. This can then help decrease the deflection of the substrate when loaded in tension.

3a Methodology – Rounded Tools

Lastly, relation between tensile stress and tool radius was explored. The same samples from the first simulations of the dovetail design were re-run after a 0.01in radius was applied to the bottom corners of the dovetail (Figure 33).

3b Results – Rounded Tools

The last study was limited to offset depths of 0 and 1/32” and angles of 20°, 40°, 60°, 80°, and 100° due to the results seen in the previous experiments. Figure 34 shows the results for the rounded tool tips follows a similar trend as the sharp tools.

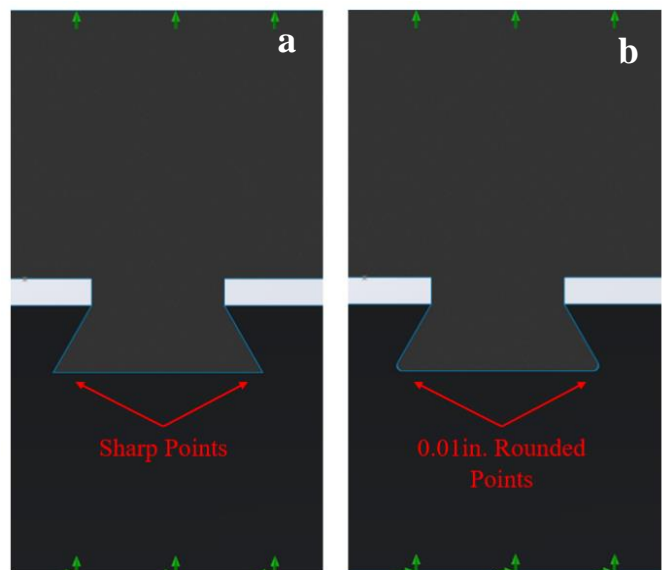


Figure 33. (a) Sharp tool point vs. (b) rounded tool

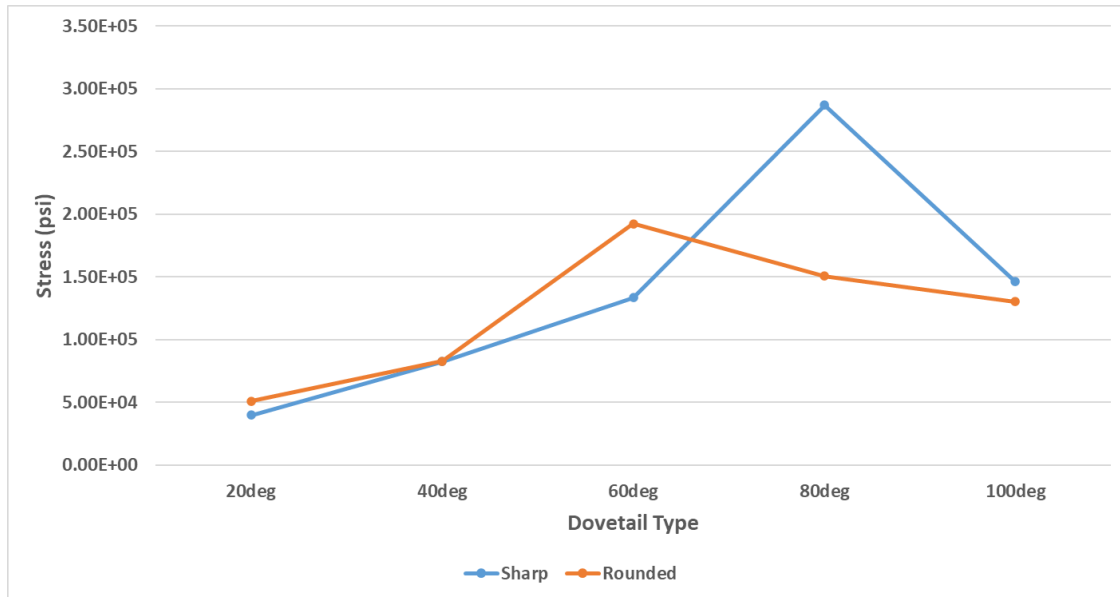


Figure 34. Maximum stress of sharp vs. rounded tool tips at 0in. offset

Differences are only seen with the 60° and 80° samples. The 60° sample sees a 59,000psi increase in stress while the 80° has an observed 136,400psi decrease in stress. This difference could be due to a shift in the peak stress due to the rounding of the tool tips. While these values are large, it is difficult to say if there is a difference between the two tool types due to the 20°, 40°, and 100° samples of each tool being remarkably close to one another.

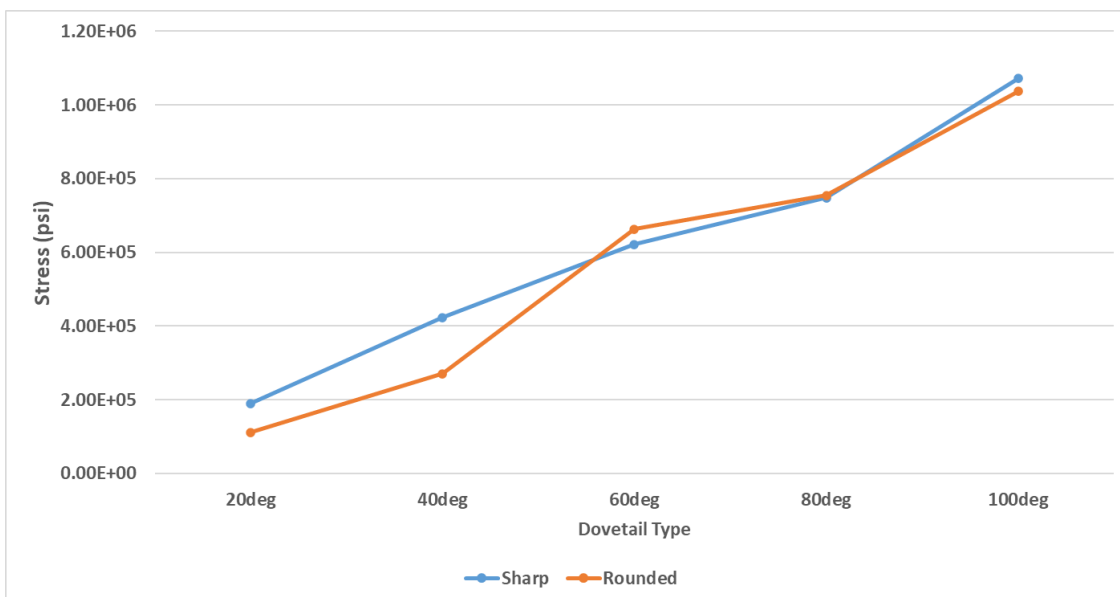


Figure 35. Maximum stress of sharp and rounded tool tips at 1/32in. offset

It is difficult to evaluate a difference between the 0in. offset values since the values seen with the 1/32in. trend close together (Figure 35). At each dovetail angle, a significant difference is not presented between the two tool types. Overall, this study provides evidence that there is a small to negligible difference between tools with sharp tips and those with rounded tips. From a manufacturing standpoint, this is beneficial because tools with rounded tips experience a longer tool life than those with sharp tips. Additionally, as soon as a sharp tipped tool is used, it becomes a rounded tip due to wear.

3.2.2 Lollipop Design

1a Methodology – Radius Change

The primary experiment of the Lollipop Design considers how changes in tool radius for a lollipop style cutter affects the overall tensile stress of the assembly. In this experiment, the width of the channel (1/4in.) and depth of the channel (1/8in.) remained constant. All radii on the vertical sides of the channel remained coincident with the top and bottom of the channel. The radii were changed by altering the “angle” of the arc. The radii are in increments of 22.5°, 45°, 90°, 135°, and 180° (Figure 36).

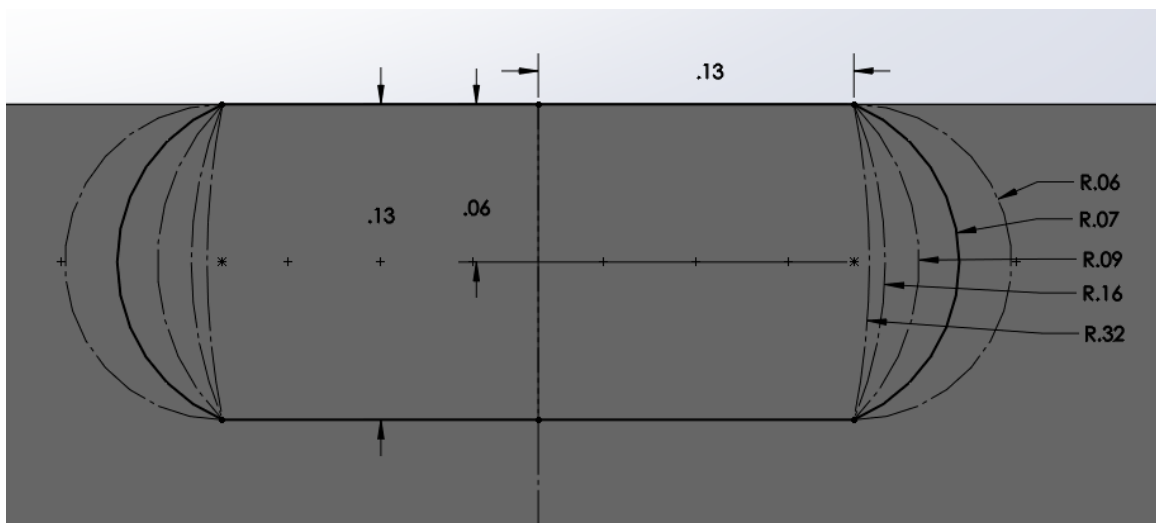


Figure 36. Drawing of lollipop cutter with varying radii side walls

1b Results – Radius Change

From this analysis, a clear trend can be seen from the change of the tool radius. Figure 37 shows an increasing linear trend of tensile stress when the radius increases from 0.06in.

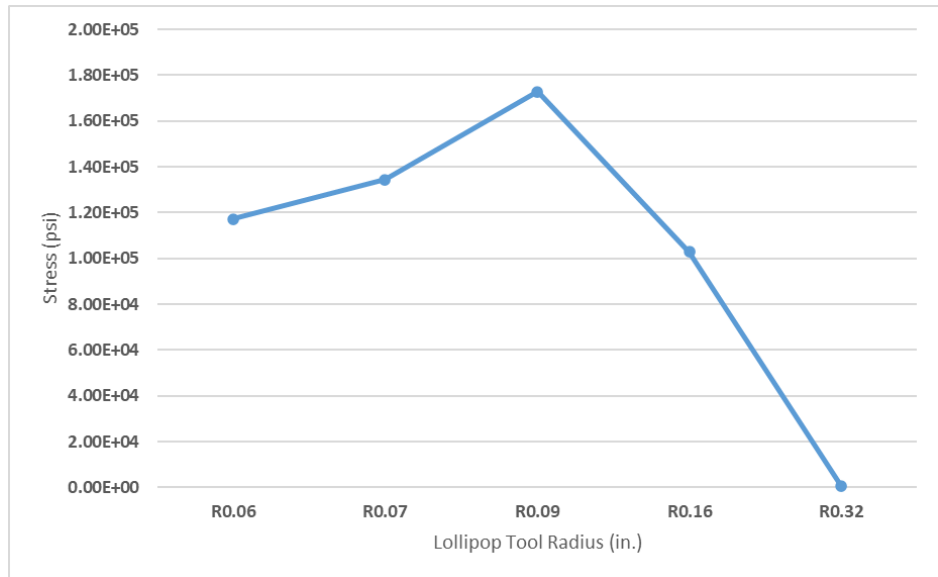


Figure 37. Maximum stress vs. tool radius

towards 0.09in. After a radius of 0.9in. a sharp decline in tensile stress is seen when the tool radius approaches 0.32in., leaving almost a straight wall on the side of the channel. This is to be expected because in this experiment the height of the channel remains constant. Therefore, as the radius of the arc increases, the side of the channel approaches perpendicular to the surface. This study provides evidence that an optimal value for the tool radius to maximize the stress, would appear to be approximately in the 0.09in. range.

2a Methodology – Stepmover Change

The second experiment held the radius of the lollipop tool constant at 1/16in. while changing the stepover distance. The width and depth remained constant (1/4in.x1/8in.). This allows the first sample to be made with a theoretical 180° of a spherical cutting tool. Six additional samples were made at 0.01in. stepover increments for a total of seven samples (Figure 38).

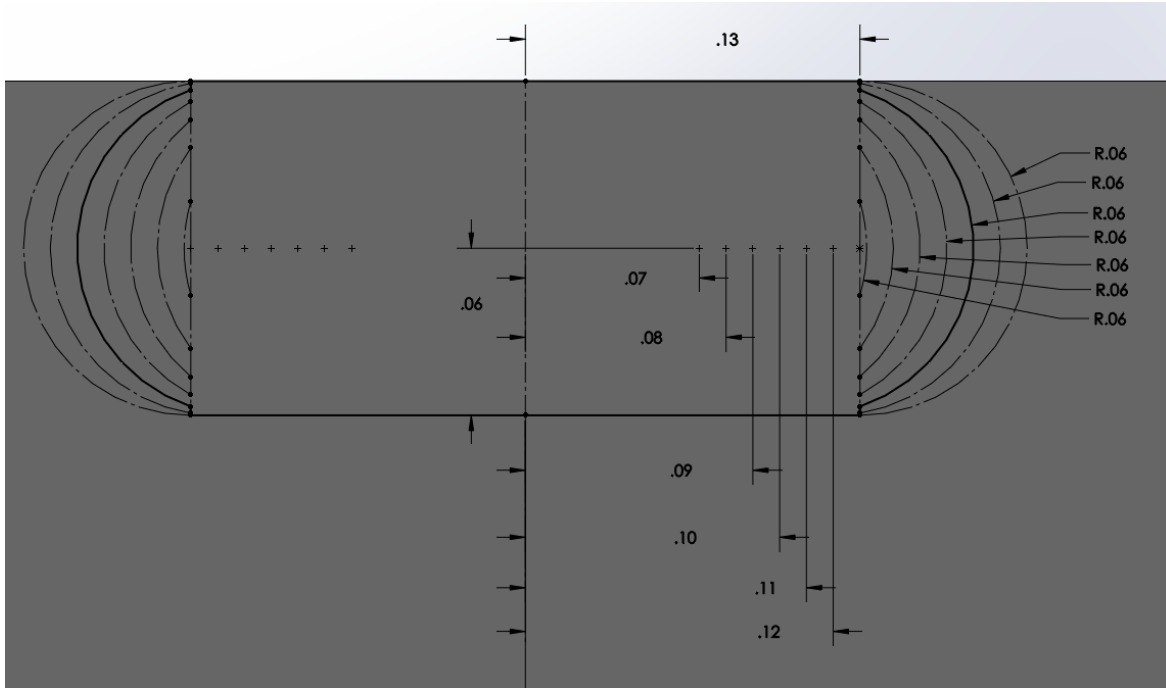


Figure 38. Drawing of side walls as stepover changes

2b Results – Stepover Change

The change in stepover results follows similar trends previously seen, providing evidence of an optimal value in stepover distance. Figure 39 shows an increasing trend of max stress as the tool is moved further away from the side of the channel until it reaches 0.04in. away from the

sidewall, decreasing thereafter. While the radius of the tool was held constant, this change in stepover ultimately changed the undercutting geometry of the root structure. As the tool stepped further away from the side of the channel, the

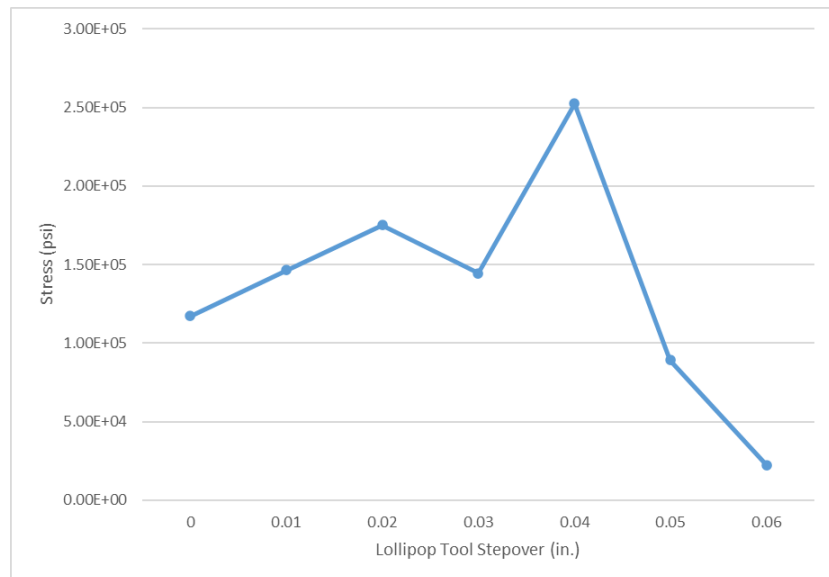


Figure 39. Maximum stress vs. tool stepover

area of the undercut geometry decreased. This study provides evidence that an optimal value for the tool stepover to maximize the stress, would appear to be approximately in the 0.04in. range.

3.2.3 Thread Design

1a Methodology – Constant Channel

Additional experiments were simulated using a channel that was a threaded hole; a 1/4in.-20 thread design was used. The first experiment investigates how the starting location of the threads (top of channel or bottom of the channel) effects the tensile stress of the system. In this study, channel dimensions were held at 1/4in. wide by 1/8in. deep. Samples were made with 1 thread starting at either the top or bottom of the channel and then adding additional threads for more samples (Figure 40).

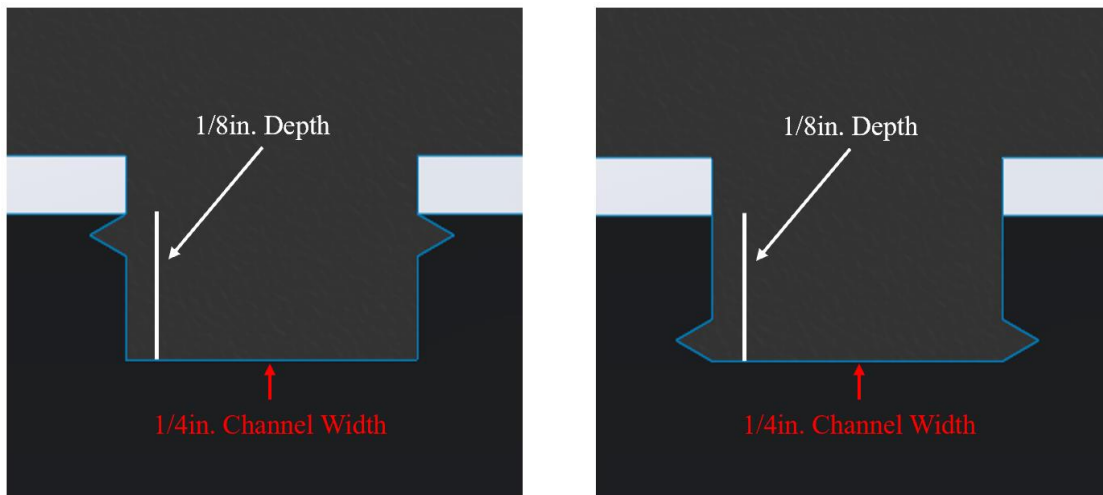


Figure 40. (a) Single top-down thread vs. (b) single bottom-up thread

1b Results – Constant Channel

When using one thread, there is no difference between the stresses withstood by the system (Figure 41). Once a second thread is added to the system, starting from the bottom provides a higher withstood stress. While there is a difference in stresses when using two threads, both the top-down approach and the bottom up approach begin to converge as a third thread is added. When adding threads in a bottom-up design, there is more substrate material

above the threads than the top-down method since the third thread ends with a small amount of vertical wall above. This design may then follow similar results to the dovetail depth test showing minimal or negligible benefits of increasing the distance between the depth of the root structure and the top of the substrate (Figure 31).

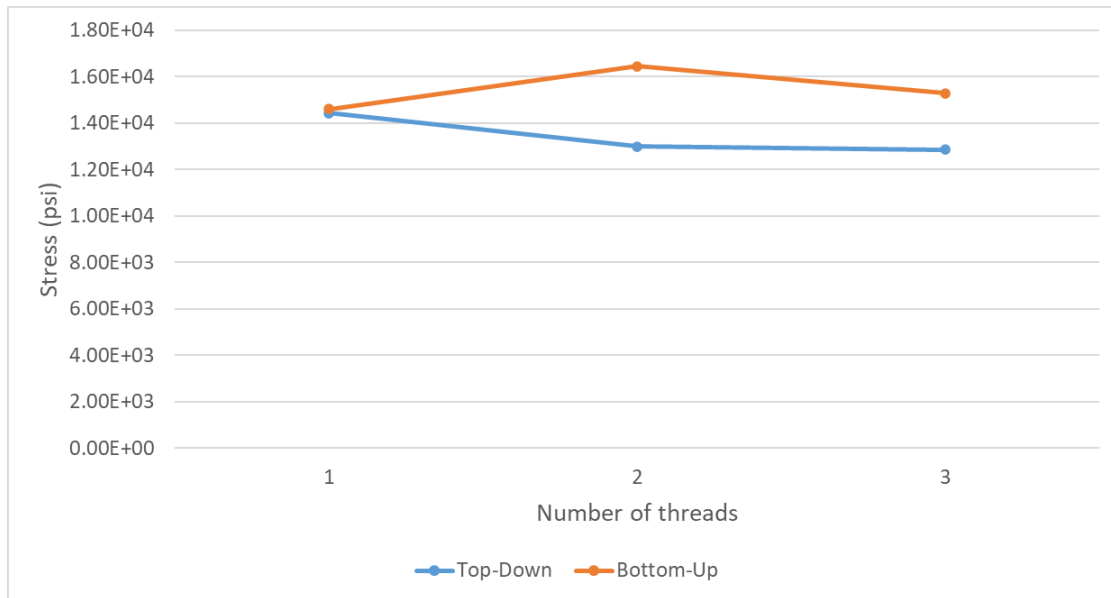


Figure 41. Stress seen in plastic between threads of a top-down vs. bottom-up approach

2a Methodology – Number of Threads

The next test was run to see if the number of threads influenced the stresses withstood by the assembly. For this study, channel width (1/4in.) remained constant on all studies. However, for this study the channel was only as deep as the number of threads being used (Figure 42). Samples were run with 1-5 threads.

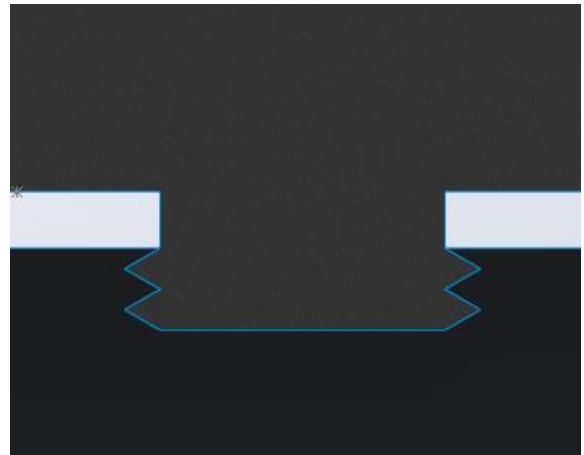


Figure 42. Two thread tensile test

2b Results – Number of Threads

While the testing method remained constant, displacement to a set distance rather than at a certain force until failure, the results seen in Figure 43 do not match the expectation. The previous FEA models presented increasing stress trends as the area of the root structure geometry increased until a certain transition point.

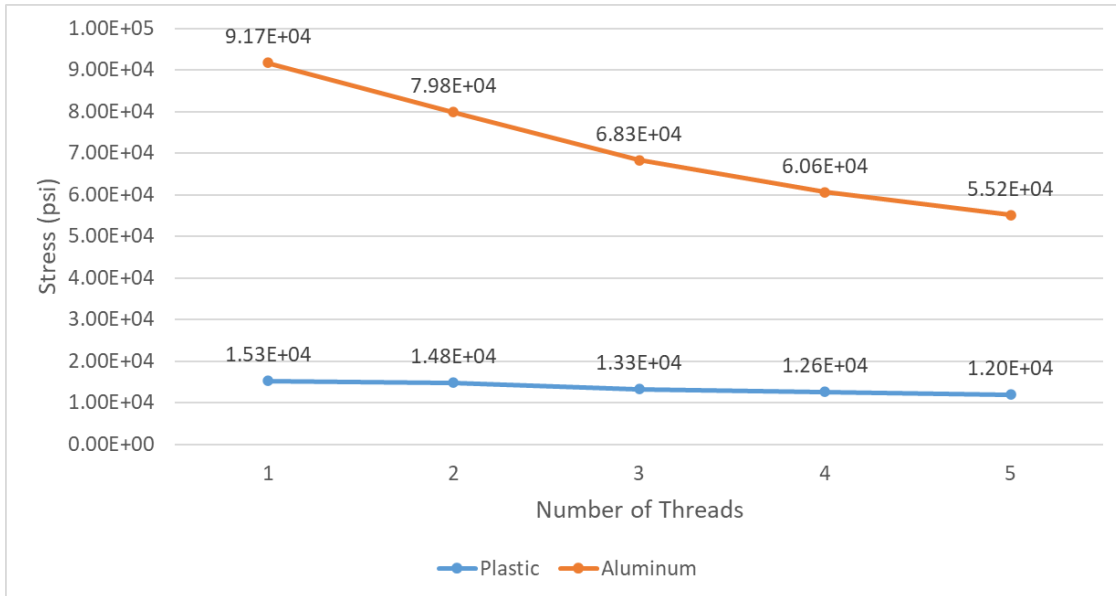


Figure 43. Stress in aluminum substrate and plastic as number of threads increases

The trend in Figure 43 would be accurate if the force was held constant. It is difficult to determine if increasing the threads leads to an increase in the tensile stress withstood by the system. Theoretically, an increase in the number of threads should increase the maximum stress withstood. Additional simulations should be run to confirm this; however, this thesis does not investigate this due to time limitations.

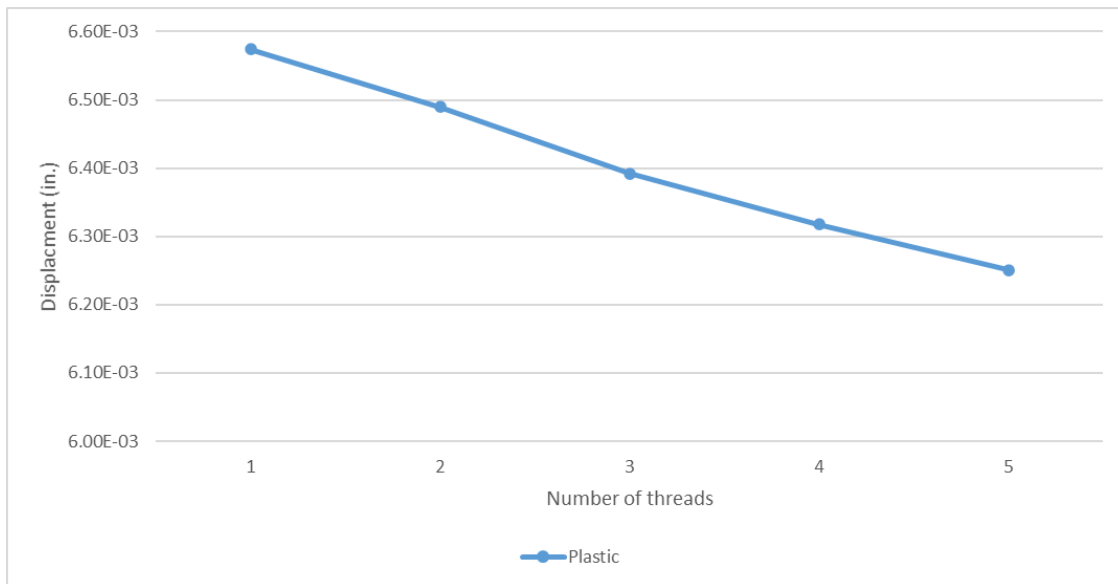


Figure 44. Displacement as the number of threads increase

The displacement prior to failure may provide another method for determining success (Figure 44). This method uses the displacement of the plastic to classify good vs. bad designs as the ability to hold two or more parts together is paramount in any joining method. This method is more advantageous to parts that need higher dimensional stability and would not want a large displacement prior to failing.

3a Methodology – Thread Location

The final experiment explored how the location of the threads may impact the tensile stresses. For this experiment, samples were created where threads were on both sides of the channel (dual threads), on exterior surfaces only, and on interior surfaces only (Figure 44). This experiment follows the same setup of channel size and number of threads used as the previous experiment.



Figure 45. (a) Dual threads vs. (b) exterior threads vs. (c) interior threads

3b Results – Thread Location

Figure 46 presents similar trends seen in the previous experiment with diminishing stresses in the aluminum as the number of threads increases. However, for this experiment the data is compared across sample groups at each thread level rather than between thread levels.

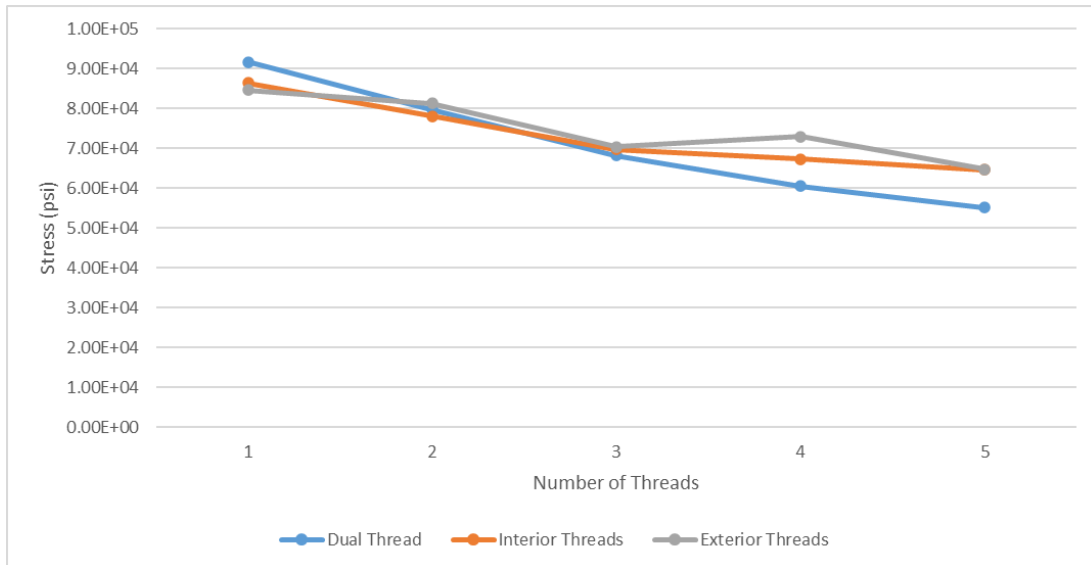


Figure 46. Maximum stress as thread location changes

From the results, all three thread locations follow a similar trend and can all withstand similar stresses prior to failure at all thread levels, providing no evidence for an optimal thread location. To classify what design performs better, an investigation of the displacement presents more promising results than the stress analysis (Figure 47). When using one thread, there is no significant difference between the three thread locations. As the number of threads increase, the difference between the three thread locations becomes more evident. The exterior threads maintain the same displacement values as the number of threads increases. This is contrary to the other two data sets that showed decreasing displacement as the number of threads increased. Using threads on both sides of the channel results in the smallest displacement, followed by the interior threads then the exterior threads. It is hypothesized that the interior threads perform better than the exterior threads due to the clamping effect; as the plastic cools, the material is pulled into the interior threads while being pulled out of the exterior threads. Using threads on both sides of the channel provides a decrease in the overall displacement but increases the machining time. The dual thread data set has the steepest linear trend, showing that increasing

the number of threads has more of an effect in the dual thread design over the interior and exterior thread designs. Due to time limitations, samples were only run up to five threads.

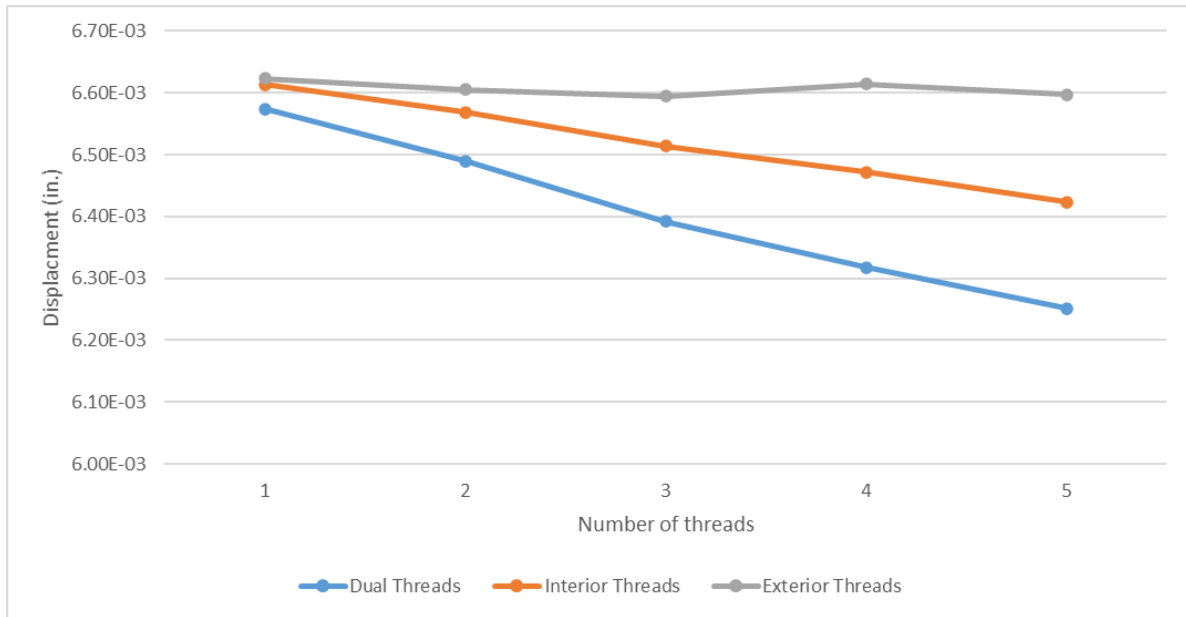


Figure 47. Change in displacement as the number of threads and thread location change

CHAPTER 4. CONCLUSIONS AND FUTURE WORK

This chapter summarizes the findings of this research, discusses the shortcomings of the work, and discusses future areas of research. This chapter is broken down into two main sections: Conclusions and Limitations and Future Work.

4.1 Conclusions

This study analyzed the joining of two different materials through the use undercutting root structures to create a multi-material structure. A baseline of tensile strength of an ABS-CF printed part is set at 2,746psi when printed at 250°C. It was found that using a temperature of 250°C resulted in prints with the highest strength across the tested temperatures. This was then used as the baseline for the remaining experiments. The findings show that using a 270° Undercutting End Mill (Lollipop cutter) provides the strongest root structure with a mean strength of 29,959psi. While the lollipop root structure had the highest mean value, it did not hold a statistical difference from the 20° dovetail, t-slot, and threaded root structure designs. In the third experiment, the substrate and print temperatures were investigated to see if there was an effect on the shear strength of the plastic portion of the multi-material structure. It was shown that at low substrate temperatures a higher printing temperature leads to higher shear strength. It also shows that as the substrate temperature increases, the shear strength increases and the printing temperature has a diminishing effect. When the substrate was heated to 100°C, there was no statistical difference between parts printed at the different print temperatures with the mean values falling between 2,728-2,871psi.

The last part of this study used FEA simulations to evaluate what aspects of the root structure geometry affect the stress of the multi-material systems. When using a dovetail for the root structure geometry, it was shown that strength increased as the included angle of the

dovetail approaches 80° then has diminishing benefits thereafter. As the depth of the dovetail geometry increases into the substrate, there does not appear to be any effect on tensile properties. However, under shear loading, increasing the depth of the root structure to $1/32$ in. away from the substrate surface led to an increase in shear stress withstood before failure. It then shows decreasing benefit as the depth continues to increase. The last section of the dovetail design provides evidence that there is no difference between using sharp tools and rounded tools. Next, this analysis looked at the use of undercutting end mills, called lollipop cutters in this study. There was evidence of an upwards linear trend as the radius of the undercutting end mill increased towards 0.09in. but then sharply decreases thereafter. As the tool radius was held constant, evidence is presented of an increasing linear trend as the tool is displaced away from the side of the channel up to 0.4in. but then sharply decreased thereafter. The final study considers several aspects of creating a threaded root structure. An analysis of a top-down vs. bottom-up threading of the channel shows that the starting location of the threads does not influence the stress of the part. Next, the number of threads was increased one at a time and the stress results were found to contradict the expectation, therefore, an analysis of the displacement of the sample material was proposed. Using a displacement criterion for the final two experiments, it was found that increasing the thread number decreased the displacement of the sample material. Finally, it was found that having external threads was less effective than having internal threads and using threads on both the interior and exterior walls lead to the smallest displacement and had decreasing displacement as the number of threads increases.

This thesis provided a new joining method between a metallic substrate and an additively manufactured polymer part without the use of adhesives or fasteners. This work presented evidence that the use of a root structure in a closed loop provides a strong joining method. While

different root structure geometries were tested, the mean strength of the lollipop geometry resulted in the highest mean strength. However, large variability resulted in inconclusive results, requiring more testing to determine an optimal design. Evidence was presented for the positive effects of increasing either the substrate or print temperature to improve the primary interlaminar bond. Additionally, beneficial root structure characteristics were provided using FEA modeling. This work can be applied to areas such as: 1) adding complex plastic layer/features to machined metal parts in-envelope without adding additional assembly steps, 2) creating casting patterns on interchangeable metal platters, or 3) mold patters for composite manufacturing on a metal substructure.

4.2 Limitations and Future Work

This research holds several limitations and avenues for future work that can be addressed in other research. The first limitation comes from the materials used during this research. For the substrate material, 6061 aluminum was used due its prevalence and ABS-CF was used due to its availability and printability. Additionally, the “clamping effect” hypothesized due to the contraction of the AM material was utilized in this study but it was not quantified. Future work could investigate this effect and provide design suggestions that relates to this effect. In this investigation, only print temperature was used during the manufacturing of the tensile testing samples but alternative temperatures were not tested in the tensile models. Additional research might identify if there is a relationship between the tensile strength of the root structure and the temperature it is printed at. This study physically tests only five different root structures and theoretically investigates many more via FEA simulations. Future research can investigate the designs from the FEA models in this study and test the physical models to verify the FEA results. Additionally, work can be completed to develop more FEA models and tests for alternative root structure designs. Along with a limited physical testing of root structures, only one profile of the

root structure (1in. square) was used. More work could investigate if the profile of the root structure leads to a better root structure with respect to tensile strength, root strength, displacement perpendicular to the substrate surface, as well as displacement parallel to the substrate surface. Lastly, this study begins to lay the groundwork for bonding multi-material via an undercutting root structure. From this work and future work, a programming model can be developed for the use of design engineers to help design for root structures when creating multi-material structures. This program could allow for the designer to input items like the thickness of the substrate as well as the substrate material and the material and design of the AM part and expected loading forces to be added as well. From there, the program should output a root structure geometry and a root structure profile that would allow for the multi-material system to withstand the estimated forces or inform the designer that the design will not work as it is currently designed.

REFERENCES

- [1] Z. Zhu, V.G. Dhokia , A. Nassehi, and S.T. Newman “A review of hybrid manufacturing processes – state of the art and future perspectives”, *International Journal of Computer Integrated Manufacturing*, vol. 26, no. 7, pp. 596-615, 2013. DOI: 10.1080/0951192X.2012.749530
- [2] “Multi-Material Printing with Your 3D Printer: Introducing Palette+,” *mosaicmfg.com*, 2020. [Online]. Available: <https://www.mosaicmfg.com/blogs/news/multi-material-printing-with-palette-plus>. [Accessed May 25, 2020]
- [3] M. C. Frank, IE 545. Class Lecture, Topic: “Selective Laser Sintering (SLS), Direct Metal Laser Sintering (DMLS), Selective Laser Melting (SLM), and Election Beam Melting (EBM).” Department of Industrial and Manufacturing Systems Engineering, Iowa State University, Ames, IA, Spring 2019.
- [4] K. P. Rajurkar, D. Zhu, J. A. McGeough, J. Kozak, and A. De Silva, “New Developments in Electro-Chemical Machining,” *CIRP Annals*, vol. 48, no. 2, pp. 567-579, 1999. DOI: [https://doi.org/10.1016/S0007-8506\(07\)63235-1](https://doi.org/10.1016/S0007-8506(07)63235-1)
- [5] M. Rivette, J-Y. Hacoët, and P. Mognol, “A graph-based methodology for hybrid rapid design,” *Journal of Engineering Manufacture*, vol. 221, no. 4, Apr. 1, pp. 685-697, 2007. DOI: <https://doi.org/10.1243%2F09544054JEM666>
- [6] M. C. Frank, IE 545. Class Lecture, Topic: “Rapid Prototyping and Manufacturing (RP&M): Background.” Department of Industrial and Manufacturing Systems Engineering, Iowa State University, Ames, IA, Spring 2019.
- [7] G. Manogharan, R. A. Wysk, and O. L. A. Hartsson, “Additive manufacturing-integrated hybrid manufacturing and subtractive processes: economic model and analysis,” *International Journal of Computer Integrated Manufacturing*, vol. 29, no. 5, pp. 473-488, 2016. DOI: <https://doi.org/10.1080/0951192X.2015.1067920>
- [8] M. C. Frank, F. Peters, X. Lou, F. Meng, and J. E. Petrzela, “A Hybrid Rapid Pattern Manufacturing System for Sand Castings,” *Solid Freeform Fabrication Symposium*, Aug. 3-5, 2009, pp. 35-46.
- [9] N. Chen and M. C. Frank, “Process planning for hybrid additive and subtractive manufacturing to integrate machining and direct energy deposition,” *Procedia Manufacturing*, vol. 34, pp. 205-213, 2019. DOI: <https://doi.org/10.1016/j.promfg.2019.06.140>
- [10] A-K. Reichler, R. Gerbers, P. Falkenberg, E. Türk, F. Dietrich, T. Vietor, and K. Dröder, “Incremental Manufacturing: Model-based part design and process planning for Hybrid Manufacturing of multi-material parts,” *Procedia CIRP*, vol. 79, pp. 107-112. DOI: <https://doi.org/10.1016/j.procir.2019.02.020>

- [11] M. C. Frank, R. A. Wysk, and S. J. Joshi, "Rapid Planning for CNC Milling – A New Approach for Rapid Prototyping," *Journal of Manufacturing Systems*, vol. 23, no. 3, pp.242-255, 2004. DOI: [https://doi.org/10.1016/S0278-6125\(04\)80037-2](https://doi.org/10.1016/S0278-6125(04)80037-2)
- [12] H. Srinivasan, "Automated Model Processing and Localization of Additively Manufactured Parts for Finish Machining," PhD Dissertation, North Carolina State University, Raleigh, NC, 2016
- [13] K. L. Basinger, C. B. Keough, C. E. Webster, R. A. Wysk, T. M. Martin, and O. L. Harrysson, "Development of a modular computer-aided process planning (CAPP) system for additive-subtractive hybrid manufacturing of pockets, holes, and flat surfaces," *The International Journal of Advanced Manufacturing Technology*, vol. 96, Feb. 22, pp. 2407-2420, 2018. DOI: <https://doi.org/10.1007/s00170-018-1674-x>
- [14] J. Ruan, K. Eiamsa-ard, and F. W. Liou, "Automatic Process Planning and Tool Path Generation of Multiaxis Hybrid Manufacturing System," *Journal of Manufacturing Processes*, vol. 7, no. 1 pp. 57-68, 2005.
- [15] H. ElMaraghy, and M. Moussa, "Optimal platform design and process plan for managing variety using hybrid manufacturing," *CIRP Annals*, vol. 68, no. 1, pp. 443-446, 2019. DOI: <https://doi.org/10.1016/j.cirp.2019.03.025>
- [16] B. Krassenstein. "BAAM 3D Printer Gets Major Upgrade - Prints 100 Lbs of Material Per Hour & More" *3DPrint.Com*, Mar. 19, 2015. Available: 3dprint.com/51109/baam-3d-printer-2/. [Accessed Feb. 8, 2020]
- [17] C. E. Duty, V. Kunc, B. Compton, B. Post, D. Erdman, R. Smith, R. Lind, P. Lloyd and L. Love, "Structure and mechanical behavior of Big Area Additive Manufacturing (BAAM) materials," *Rapid Prototyping Journal*, vol. 23, no. 1, p. 181-189, 2017. DOI: <https://doi.org/10.1108/RPJ-12-2015-0183>
- [18] Q. Sun, G. M. Rizvi, C. T. Bellehumeur, and P. Gu, "Effect of processing conditions on the bonding quality of FDM polymer filaments," *Rapid Prototyping Journal*, vol. 14, no. 2, pp. 72-80, 2008. DOI: <https://doi.org/10.1108/13552540810862028>
- [19] A. C. Abbott, G. P. Tandon, R. L. Bradford, H. Koerner, and J. W. Baur, "Process-structure-property effects on ABS bond strength in fused filament fabrication," *Additive Manufacturing*, vol. 19, pp. 29-38, 2018. DOI: <https://doi.org/10.1016/j.addma.2017.11.002>
- [20] Jo, W., O. Kwon, and M. Moon, "Investigation of influence of heat treatment on mechanical strength of FDM printed 3D objects," *Rapid Prototyping Journal*, vol. 24, no. 3, 637-644, 2018. DOI: <https://doi.org/10.1108/RPJ-06-2017-0131>
- [21] A. Roschli, K. T. Gaul, A. M. Boulger, B. K. Post, P. C. Chesser, L. J. Love, F. Blue, M. Borish, "Designing for Big Area Additive Manufacturing," *Additive Manufacturing*, vol. 25, pp. 275-285, 2019. DOI: <https://doi.org/10.1016/j.addma.2018.11.006>

- [22] C. E. Duty, T. Drye, and A. Franc, "Material Development for Tooling Applications Using Big Area Additive Manufacturing (BAAM)," Oak Ridge National Laboratory, Oak Ridge, TN, Tech. Report. ORNL/TM-2015/78 ED2701000; CEED492, 1 Mar. 2015
- [23] L. J. Love, V. Kunc, O. Rios, C. E. Duty, A. M. Elliott, B. K. Post, R. J. Smith, and C. A. Blue, "The importance of carbon fiber to polymer additive manufacturing," *Journal of Materials Research*, vol. 29, no. 17, Sep 14, pp. 1893-1898, 2014. DOI: <https://doi.org/10.1557/jmr.2014.212>
- [24] P. C. Chesser, R. F. Lind, B. K. Post, A. C. Roschli, L. J. Love, and K. T. Gaul, "Using Post-tensioning in Large Scale Additive Parts for Load Bearing Structures," In Proc. 29th Annual International Solid Freeform Fabrication Symposium, , Austin, TX, Aug. 1, 2018, N. p.
- [25] A. Garg, A. Bhattacharya, and A. Batish, "Chemical vapor treatment of ABS parts built by FDM: Analysis of surface finish and mechanical strength," *The International Journal of Advanced Manufacturing Technology*, vol. 89, no. 5, pp. 2175-2191, 2017. DOI: <https://doi.org/10.1007/s00170-016-9257-1>
- [26] S. Shaffer, K. Yang, J. Vargas, M. A. Di Prima, and W. Voit, "On reducing anisotropy in 3D printed polymers via ionizing radiation," *Polymer*, vol. 55, no. 23, Nov. pp. 5969-5979, 2014. DOI: <https://doi.org/10.1016/j.polymer.2014.07.054>
- [27] G. Li, J. Zhao, W. Wu, J. Jiang, B. Wang, H. Jiang, and J. Ying Hsi Fuh, "Effect of Ultrasonic Vibration on Mechanical Properties of 3D Printing Non-Crystalline and Semi-Crystalline Polymers," *Materials*, vol. 11, no. 5, N. p., 2018. DOI: <https://doi.org/10.3390/ma11050826>
- [28] A. Roschli, C. E. Duty, J. Lindahl, B. K. Post, P. C. Chesser, L. J. Love, and K. T. Gaul, "Increasing Interlaminar Strength in Large Scale Additive Manufacturing," In. Proc. 29th International Solid Freeform Fabrication Symposium, Austin, TX, 2018, N. p.
- [29] V. Kishore, A. Nycz, J. Lindahl, C. E. Duty, C. Carnal, and V. Kunc, "Effect of Infrared Preheating on the Mechanical Properties of Large Format 3D Printed Parts," In. Proc. 30th Annual International Solid Freeform Fabrication Symposium (SFF 2019), Austin, TX, 2019, N. p.
- [30] S. C. Partain, "Fused Deposition Modeling with Localized Pre-Deposition Heating Using Forced Air," M. S. thesis, Montana State University, Bozeman, MT, 2007.
- [31] A. K. Ravi, A. Deshpande, and K. H. Hsu, "An in-process laser localized pre-deposition heating approach to inter-layer bond strengthening in extrusion based polymer additive manufacturing," *Journal of Manufacturing Processes*, vol. 24, pp. 179-185, 2016. DOI: <http://dx.doi.org/10.1016/j.jmapro.2016.08.007>

- [32] A. Bandyopadhyay, and B. Heer, “Additive manufacturing of multi-material structures,” *Materials Science and Engineering: R: Reports*, vol. 129, pp. 1-16, 2018. DOI: <https://doi.org/10.1016/j.mser.2018.04.001>
- [33] K. Arcaute, N. Zuverza, B. Mann, and R. Wicker, “Multi-material Stereolithography: Spatially-controlled Bioactive Poly(Ethylene Glycol) Scaffolds for Tissue Engineering,” In Proc. 18th Annual Solid Freeform Fabrication Symposium, Austin, TX, 2007, pp. 458-469
- [34] M. Silva, R. Felismina, A. Mateus, P. Parreira, and C. Malça, “Application of a Hybrid Additive Manufacturing Method to Produce a Metal/Polymer Customized Dental Implant.” *Procedia Manufacturing*, vol. 12, pp. 150-155, 2017. DOI: <https://doi.org/10.1016/j.promfg.2017.08.019>
- [35] D. D. Gu, W. Meiners, K. Wissebach, and R. Poprawe, “Laser additive manufacturing of metallic components: materials, processes and mechanisms,” *International Materials Reviews*, vol. 53, no. 7, Nov. 12, pp. 133-164, 2013. DOI: <https://doi.org/10.1179/1743280411Y.0000000014>
- [36] M. L. Griffith, L. D. Harwell, J. T. Romero, E. Schlienger, C. L. Atwood, and J. E. Smugeresky, “Multi-material Processing by LENS,” 1997 International Solid Freeform Fabrication Symposium, N. p.
- [37] J-W. Choi, H-C. Kim, and R. Wicker, “Multi-material stereolithography,” *Journal of Materials Processing Technology*, vol. 221, no. 3, Mar. 1, pp. 318-328, 2011, DOI: <https://doi.org/10.1016/j.jmatprotec.2010.10.003>
- [38] R. Stott, “Synthesis Design + Architecture Utilizes Gradient 3-D Printing in “Durotaxis Chair”,” *archdaily.com*, 2015. [Online]. Available: <https://www.archdaily.com/610939/synthesis-design-architecture-utilizes-gradient-3-d-printing-in-durotaxis-chair>. [Accessed May 23, 2020].
- [39] “Dissimilar Materials Joining,” *ewi.org*, July 27, 2012. [Online]. Available: <https://ewi.org/dissimilar-materials-joining/>. [Accessed May 24, 2020].
- [40] PolyOne, *GLS Overmolding Guide*, 2004.
- [41] Protolabs, *Design Essentials for Injection Molding*, 2018.
- [42] A. Albert, W. Zorn, W-G. Drossel, W. Nendel, “Process Combination of Hydroforming and Injection Moulding for the In Situ Manufacturing of Metal and Plastic Composite Structures,” *Materials and Science Forum*, vols. 825-826, pp. 522-529. 2015. DOI: [10.4028/www.scientific.net/MSF.825-826.522](https://doi.org/10.4028/www.scientific.net/MSF.825-826.522)

- [43] A. Albert, W. Zorn, M. Layer, W-G. Drossel, D. Landgrebe, L. Kroll, W. Nendel, “Smart Processing Combination for Aluminum/Plastic Hybrid Components,” *Technologies for Lightweight Structures*, vol. 1, no. 2, pp. 44-53, 2017. DOI: <http://dx.doi.org/10.21935/tls.v1i2.91>
- [44] ElringKlinger, *Lightweight Technologies*, 2020.
- [45] (ASTM), Standard Test Method for Tensile Properties of Plastic, 2014
- [46] H. Bhavnagarwala, “The Perfect ABS Print & Bed Temperature,” all3dp.com, Nov. 25, 2019. [Online]. Available: <https://all3dp.com/2/abs-print-bed-temperature-all-you-need-to-know/>. [Accessed: Feb. 10, 2020].
- [47] M. Tyson, “Advanced Guide to Printing ABS Filament,” 3dprintingsolutions.com, June 4, 2018. [Online]. Available: <https://www.3dprintingsolutions.com.au/News/Australia/how-to-3d-print-abs-filament>. [Accessed: Feb. 10, 2020].
- [48] “How to Succeed When Printing With ABS,” matterhackers.com, Apr. 22, 2014. [Online]. Available: <https://www.matterhackers.com/articles/how-to-succeed-when-printing-with-abs>. [Accessed: Feb. 10, 2020].
- [49] C. Ajinjeru, V. Kishore, P. Liu, J. Lindahl, A. A. Hassen, V. Kunc. B. Post, L. Love, and C. Duty, “Determination of melt processing conditions for high performance amorphous thermoplastics for large format additive manufacturing,” *Additive Manufacturing*, vol. 21, pp. 125-132, 2018. DOI: <https://doi.org/10.1016/j.addma.2018.03.004>
- [50] S. Larson, “Hybrid Manufacturing with Multi-Material Structures Research Journal,” Slater Laboratory for Advanced Manufacturing, Ames, Iowa, unpublished
- [51] A. B. Khorasani. “Developing a new test method for evaluating substrate/deposited interfacial bonding strength of part manufactured with hybrid manufacturing”, unpublished.